

Solvent-Oriented Structure Diversity, Sequential SCSC and Low-Temperature Transformation in Cd-Coordination Polymers: Unique Turn-On-Off Sensing to Fe³⁺

Zhen Zhang,^a Jie Zhou,^{*,a} Xue Chen,^a Tong Yan,^a Hanxu Sun,^a Lin Du,^a Qihua Zhao^{*,a}

^aKey Laboratory of Medicinal Chemistry for Natural Resource, Ministry of Education and Yunnan Province, Yunnan Characteristic Plant Extraction Laboratory, School of Chemical Science and Technology, Yunnan University, Kunming, 650500, P. R China

*Corresponding Author

Jie Zhou*

E-Mail: zhoujie@ynu.edu.cn

Qi-Hua Zhao*

E-Mail: qhzhao@ynu.edu.cn

Contents

1. Experimental section

1.1 Materials and instruments

1.2 X-ray Crystallographic Measurement

1.3 Synthesis of Cd-CPs

1.4 Fluorescence Sensing Experiments

2. Detailed structural description of the Cd-CPs

3. Supporting Figure

Fig. S1 Structure of **Cd-1'**

Fig. S2 Diagrams comparing the difference of structural component of **Cd-1** and **Cd-1'**

Fig. S3 Distance between the backbone of terrace layers of **Cd-1** and **Cd-1'**

Fig. S4 Structure of **Cd-2**

Fig. S5 Structure of **Cd-3**

Fig. S6 Topology analysis of **Cd-3**

Fig. S7 Structure of **Cd-4**

Fig. S8 Structure of **Cd-5**

Fig. S9 Structures of **Cd-6**

Fig. S10 Structure of **Cd-7**

Fig. S11 Simulated and as-synthesized PXRD patterns for **Cd-CPs**.

Fig. S12 Twisting of the alkoxy chain in the different conformations of **Cd-CPs**.

Fig. S13 Dihedral angles between pyridine rings in 3-bpdb of **Cd-CPs**.

Fig. S14 SCSC transformation PXRD patterns for **Cd-1'** to **Cd-2** and **Cd-3**.

Fig. S15 SCSC transformation PXRD patterns for **Cd-5** to **Cd-7**.

Fig. S16 SCSC transformation PXRD patterns for between **Cd-5** and **Cd-2**.

Fig. S17 Scanning electron microscope images of **Cd-5**, **Cd-6**, **Cd-7**.

Fig. S18 PXRD patterns of **Cd-2** and **Cd-7** immersed in aqueous solutions for 35 days.

Fig. S19 Emission and excitation spectra of *n*-BuO-H₂ip and 3-bpdb at solid-state, and **Cd-2** and **Cd-7** in aqueous solution.

Fig. S20 Emission spectra of **Cd-2** and **Cd-7** in different cations.

Fig. S21 Emission spectra of **Cd-2** immersed in aqueous solutions with Al^{3+} and Cr^{3+} at different concentrations. Fitting curve of I/I_0 vs Al^{3+} and Cr^{3+} concentration.

Fig. S22 Emission spectra of **Cd-7** immersed in aqueous solutions with Al^{3+} and Cr^{3+} at different concentrations. Fitting curve of I/I_0 vs Al^{3+} and Cr^{3+} concentration.

Fig. S23 Fluorescence emissions of **Cd-2** to Fe^{3+} within 2 cycles and 3 cycles.

Fig. S24 Emission spectra of **Cd-7** immersed in aqueous solutions with Fe^{3+} at different concentrations. Fitting curve of I/I_0 vs Fe^{3+} concentration.

Fig. S25 Selective detection of Cr^{3+} and Al^{3+} by **Cd-2** in the presence of other cations in the aqueous medium.

Fig. S26 Selective detection of Cr^{3+} and Al^{3+} by **Cd-7** in the presence of other cations in the aqueous medium.

Fig. S27 PXRD patterns of **Cd-2** and **Cd-7** after sensing Al^{3+} , Cr^{3+} and Fe^{3+} .

Fig. S28 UV-vis absorption spectrum of **Cd-2** and with the addition of Cr^{3+} , Al^{3+} and Fe^{3+} .

Fig. S29 UV-vis absorption spectrum of **Cd-7** and with the addition of Cr^{3+} , Al^{3+} and Fe^{3+} .

Fig. S30 XPS analysis of the O 1s peaks of **Cd-2** before and after immersed in the aqueous solution of Cr^{3+} , Al^{3+} , and Fe^{3+} .

Fig. S31 XPS analysis of the N 1s peaks of **Cd-2** before and after immersed in the aqueous solution of Cr^{3+} , Al^{3+} , and Fe^{3+} .

Fig. S32 XPS analysis of the O 1s peaks of **Cd-7** before and after immersed in the aqueous solution of Cr^{3+} , Al^{3+} , and Fe^{3+} .

Fig. S33. XPS analysis of the N 1s peaks of **Cd-7** before and after immersed in the aqueous solution of Cr^{3+} , Al^{3+} , and Fe^{3+} .

Fig. S34 Excitation and emission wavelength of **Cd-2** and UV-vis absorption spectrum of Cr^{3+} , Al^{3+} , and Fe^{3+} .

Fig. S35 FT-IR spectra of **Cd-1'–Cd-7**.

Fig. S36 TG curves of **Cd-1'–Cd-7**.

Fig. S37 Solid-state fluorescence spectra of **Cd-1'–Cd-7**.

4. Supporting Schemes

Scheme S1 Coordination Modes of the *n*-BuO-ip²⁻ Ligands in **Cd-1'**, **Cd-2**, and **Cd-3**.

Scheme S Schematic illustration of the PET process and the turn-on sensing of Cr³⁺, Al³⁺, and Fe³⁺ for **Cd-2** and **Cd-7**.

5. Supporting Tables

Table S1 Crystal data and structure refinement summary for **Cd-1–Cd-7**.

Table S2 Selected Bond Lengths (Å) and Angles (°) for **Cd-1–Cd-7**.

Table S3 transformation conditions.

Table S4 SCSC Comparison of the ground state energies and the transformation energy for Cd-CPs calculated at B3LYP/LANL2DZ² level.

Table S5 Fluorescent sensor for Cr³⁺ and Al³⁺ detection based on various CPs.

1. Experimental Section

1.1 Materials and instruments

Ligands of 3-bpdb and *n*-BuO-H₂ip were synthesized according to the literature.^{1, 2} Other reagents and solvents were commercially available and were used without further purification. Elemental analyses for C, H, and N were carried out with an Elementar Vario EL III analyzer. IR spectra were recorded on an FT-IR Thermo Nicolet Avatar 360 using KBr pellets in the 4000–400 cm⁻¹ region. The phase purity of the samples was investigated by powder X-ray diffraction (PXRD) measurements carried out on a Bruker D8-Advance diffractometer equipped with Cu-K α radiation ($\lambda = 1.5418 \text{ \AA}$) at a scan speed of 1 °/min. Simulation of the PXRD patterns was performed using single-crystal data and processed with the Mercury 3.9 program available free of charge through the Internet at <http://www.iucr.org>. Variable temperature powder X-ray patterns (VT-PXRD) were obtained on a Bruker D8 Venture diffractometer using Mo-K α radiation. Luminescence spectroscopy was performed on a Lengguang (Shanghai, China) F98 fluorescence spectrophotometer. Thermogravimetric analysis (TGA) data were acquired using a Mettler-Toledo simultaneous thermal analyzer from room temperature to 800 °C under an N₂ atmosphere with a heating rate of 10 °C/min. The morphology of the samples was observed using a field-emission scanning electron microscope (FE-SEM; Nova Nano SEM 450, 10 kV). X-ray Photoelectron Spectroscopy (XPS) was performed on a K-Alpha⁺ of Thermo fisher Scientific with Al K α radiation ($h\nu = 1486.6 \text{ eV}$). The ultraviolet–visible (UV–vis) spectrum was recorded with Hitachi UV-1900. Differential Scanning Calorimeter (DSC) measurement was conducted on German NETZSCH 200 F3, with a heating rate of 10 °C/min in N₂. Point symbol and topological analyses were conducted by using the TOPOS program package.³

1.2 X-ray Crystallographic Measurement

Single crystals suitable for X-ray diffraction were coated with methylsilicon oil (Urchem) on a slide glass, transferred to a polyimide film loop (MiTeGen micromount),

and then quickly mounted on the goniometer head of a Bruker D8 Venture PHOTON CMOS system equipped with a mirror monochromator, a Mo K α INCOATEC *I μ S* 3.0 micro-focus radiation source ($\lambda = 0.71073$ Å). The crystal samples were optically aligned. It is noteworthy that the data of **Cd-1'** were collected at 298 K, while **Cd-1** were collected at 100 K using an Oxford Cryostream 700 system. Especially, the crystals of **Cd-1** and **Cd-4** used for data collection were found to display non-merohedral twinning. The APEX3 software program (version 2018.7-2)⁴ was used for diffractometer control. Intensity data were integrated using the SAINT+ software.⁵ Empirical absorption correction was applied using the SADABS program.⁶ Using Olex2,⁷ the structures were solved with the SHELXT⁸ structure solution program with Intrinsic Phasing and refined with the SHELXL⁶ refinement package. In all structures, the hydrogen atoms attached to organics either originated from being fixed by stereochemistry or differential Fourier diagrams. The structures of **Cd-1**, **Cd-1'**, **Cd-3**, and **Cd-7** contain an area of disordered lattice water molecules; attempts to model them with a chemically reasonable geometry were unsuccessful. Therefore, the SQUEEZE procedure of PLATON⁹ was employed to remove the contributions of the electron density associated with water molecules from the intensity data. Because of the disordered water molecules, the positions of the corresponding hydrogen atoms could not be clearly localized. The solvent-free model and intensity data were used for the final results reported here. Likely the consequence of twinning, larger than expected residual density minimum outside metal atom locations. The highest residual electron density peaks of 2.2 eÅ⁻³ is localized 0.94 Å from Cd2 in **Cd-1**, and the highest residual electron density peaks of 1.86 eÅ⁻³ is localized 0.98 Å from Cd1 in **Cd-4**. The crystallographic data and details of the structure refinements are listed in Table S1, and the selected bond distances and angles are given in Table S2.

1.3 Fluorescence Sensing Experiments

The luminescence properties of **Cd-2** and **Cd-7** were investigated at room temperature. For the luminescence sensing of cations, the crystal samples of **Cd-2** and **Cd-7** were ground uniformly, and then the crystals were ultrasonically dispersed at a ratio of 1

mg/mL for 30 min to form a stable suspension. 2 mL of the suspension was taken in a cuvette, and the luminescence of the suspension was measured after adding different kinds of cations (0.01 M).

1.4 Synthesis of Cd-CPs

[Cd₂(3-bpdb)₂(*n*-BuO-ip)₂]_n (Cd-1).

A mixture of Cd(NO₃)₂·4H₂O (15.42 mg, 0.05 mmol), 3-bpdb (5.25 mg, 0.025 mmol), *n*-BuO-H₂ip (5.95 mg, 0.025 mmol), and DMF: H₂O (2 mL; 1:1, v:v) was sealed in a 5 mL glass reactor, heated at 115 °C for 2 days, and then cooled to room temperature. Yellow flake crystals of **Cd-1** were obtained and SC-XRD data were collected at 100 K.

[Cd(3-bpdb)(*n*-BuO-ip)]_n (Cd-1').

The First Method:

Cd-1' was prepared as the first method of **Cd-1** except that the SC-XRD data were collected at 298 K. Yield: 54% (based on 3-bpdb). Elemental analysis (%): calcd for (C₂₄H₂₂CdN₄O₅): C 51.58, H 3.97, N 10.03; Found: C 51.48, H 4.12, N 10.02.

The Second Method:

It was prepared similar to the first method except that the DMF: H₂O (2 mL; 1:1, v:v) was changed to H₂O: CH₃OH (2 mL; 2:3, v:v). Yellow flake crystals of **Cd-1'** were obtained. Yield: 58% (based on 3-bpdb).

[Cd(3-bpdb)(*n*-BuO-ip)(H₂O)]_n (Cd-2).

The First Method:

Cd-2 was prepared similar to the first method of **Cd-1** except that the DMF: H₂O (2 mL; 1:1, v:v) was changed to DMF: H₂O (2 mL; 1:3, v:v). Yellow diamond-like crystals of **Cd-2** were obtained. Yield: 50% (based on 3-bpdb). Elemental analysis (%): calcd for (C₂₄H₂₄CdN₄O₆): C 49.97, H 4.19, N 9.71; Found: C 49.89, H 4.21, N 9.82.

The Second Method: SCSC transformations.

As-synthesized **Cd-1'** were dipped in DMF: H₂O (2 mL; 1:3, v:v) at RT for 7 days, **Cd-**

2 was afford.

The Third Method: SCSC transformations.

The samples of **Cd-5** were dipped in DMF: H₂O (2 mL; 1:6, v:v) at RT for 16 days, **Cd-2** was afford.

$\{[\text{Cd}_2(\text{3-bpdb})_{2.5}(\text{n-BuO-ip})_2(\text{H}_2\text{O})] \cdot 2\text{H}_2\text{O}\}_n$ (**Cd-3**).

The First Method:

Cd-3 was prepared similar to the first method of **Cd-1** except that the DMF: H₂O (2 mL; 1:1, v:v) was changed to DMF: H₂O (2 mL; 1:6, v:v). Yellow needle-like crystals of **Cd-3** were obtained. Yield: 46% (based on 3-bpdb). Elemental analysis (%): calcd for (C₅₄H₅₅Cd₂N₁₀O₁₃): C 50.79, H 4.34, N 10.97; Found: C 50.65, H 4.38, N 10.94.

The Second Method: SCSC transformations.

Stirring crystal samples of **Cd-1'** in aqueous solution, recrystalling for two weeks at RT, **Cd-3** was formed.

$[\text{Cd}_2(\text{3-bpdb})_2(\text{n-BuO-ip})(\text{n-BuO-Hip})_2(\text{H}_2\text{O})_2]_n$ (**Cd-4**).

Cd-4 was prepared similar to the first method of **Cd-1** except that the DMF: H₂O (2 mL; 1:1, v:v) was changed to H₂O (2 mL). Colorless rod-like crystals of **Cd-4** were obtained. Yield: 39% (based on 3-bpdb). Elemental analysis (%): calcd for (C₆₀H₆₂Cd₂N₈O₁₇): C 51.77, H 8.98, N 8.05; Found: C 51.47, H 8.97, N 8.13.

$\{[\text{Cd}(\text{3-bpdb})_{0.5}(\text{n-BuO-ip})(\text{DMF})(\text{H}_2\text{O})] \cdot \text{H}_2\text{O}\}_n$ (**Cd-5**).

The First Method: SCSC transformations.

Colorless block crystals of **Cd-5** were obtained by immersing the as-made **Cd-1'** in the mother liquor (or immersed in DMF–H₂O (2 mL; 1:1, v:v) for 14 days. Elemental analysis (%): calcd for (C₂₁H₂₈CdN₃O₈): C 44.81, H 5.01, N 7.47; Found: C 44.78, H 4.89, N 7.53.

The Second Method: SCSC transformations.

As-synthesized **Cd-2** were placed in a glass reactor heated at 105 °C for 2 days, and then cooled to room temperature. Gradually precipitate colorless block crystals of **Cd-5**.

$\{[\text{Cd}_2(\text{3-bpdb})(n\text{-BuO-ip})_2(\text{H}_2\text{O})_4]\cdot\text{H}_2\text{O}\}_n$ (Cd-6).

Crystals of **Cd-5** were left in DMF–H₂O (2 mL; 1:19, v:v) at RT for 16 days, yellow block crystals of **Cd-6** were afford. Elemental analysis (%): calcd for (C₃₆H₄₄Cd₂N₄O₁₅): C 43.34, H 4.45, N 5.62; Found: C 43.24, H 4.42, N 5.68.

$[\text{Cd}(\text{3-bpdb})_{0.5}(n\text{-BuO-ip})(\text{H}_2\text{O})]_n$ (Cd-7).

The First Method: SCSC transformations.

Crystals of **Cd-5** were left in aqueous solution at RT for 0.5 hours, yellow block crystals of **Cd-7** were obtained. Elemental analysis (%): calcd for (C₁₈H₁₉CdN₂O₆): C 45.82, H 4.06, N 5.94; Found: C 45.72, H 4.21, N 5.88.

The Second Method: SCSC transformations.

The samples of **Cd-5** were placed in a constant temperature (298 K) and humidity box with a humidity of 98% for 4 hours, a color changed from light white to yellow, samples of **Cd-7** were obtained.

2. Detailed structural description of Cd-CPs

$[\text{Cd}(\text{3-bpdb})(n\text{-BuO-ip})]_n$ (**Cd-1'**). Single-crystal X-ray diffraction analysis revealed that **Cd-1** crystallizes in the triclinic space group $P\bar{1}$. The asymmetric unit consists of one Cd²⁺ ion, one 3-bpdb ligand, and one *n*-BuO-ip²⁻ anion (Fig. S1a). As illustrated in Fig. S1a, each distorted octahedral Cd²⁺ ion is coordinated by four equatorial O atoms originating from three *n*-BuO-ip²⁻ ligands and two N atoms from two 3-bpdb ligands. The Cd–O bond lengths vary from 2.272(6) to 2.402(6) Å, whereas the Cd–N bond distances are 2.325(7) and 2.349(8) Å, which are within the normal range.¹⁰ Two symmetry-related Cd²⁺ centers (Cd1 and, Cd1A) are bridged by carboxylate groups with bidentate bridging ($\mu_2\text{-}\eta^1:\eta^1$) and bidentate chelating (η^2) modes, forming a binuclear secondary building unit (SBU) of $[\text{Cd}_2(\text{COO})_4]$ with a Cd···Cd separation of 4.120 Å (Fig. S1b). The adjacent SBUs are extended by $\mu_3\text{-}(n\text{-BuO-ip}^{2-})$ linkers to generate one-dimensional (1D) ribbons along the *a* axis (Fig. S1c). The straight ribbons of 1D wireless extensions are further connected by 3-bpdb ligands, generating a two-dimensional (2D) terrace double-layered structure. Topologically, the 2D network

shows the 3,5-connected $(4^2.6)(4^2.6^7.8)$ topology with each $n\text{-BuO-ip}^{2-}$ ligand as a 3-connected node and each Cd^{2+} ion as a 5-connected node.¹¹ In addition, calculation using PLATON showed that the accessible volume for **Cd-1'** is 221.0 \AA^3 (16.6%) after the removal of the guest water molecules.

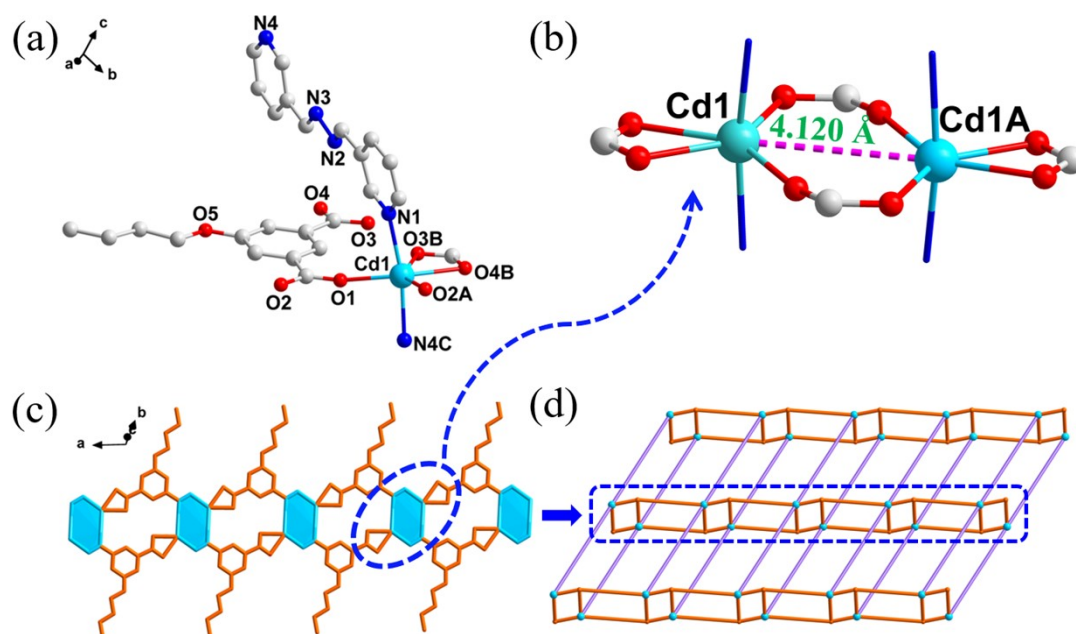


Fig. S1 (a) Coordination environment of Cd^{2+} ion in **Cd-1'** (symmetry codes: (A) $-x+3, -y+1, -z+1$; (B) $-x+2, -y+1, -z+1$; (C) $x+1, y+1, z$). (b) SBU of $[\text{Cd}_2(\text{COO})_2]$ in **Cd-1'**. (c) View of 1D $[\text{Cd}_2(n\text{-BuO-ip})_2]_n$ straight ribbon linked by $n\text{-BuO-ip}^{2-}$ anions. (d) Schematic of the 2D terrace layer of **Cd-1'** with $(4^2.6)(4^2.6^7.8)$ topology.

$[\text{Cd}_2(3\text{-bpdb})_2(n\text{-BuO-ip})_2]_n$ (**Cd-1**). When data were collected at 100 K, **Cd-1** with a significant difference in crystallographic parameters from **Cd-1'** was obtained (Table S1). Structural determination revealed that **Cd-1** crystallizes in the triclinic space group $P\bar{1}$ with the asymmetric unit consisting of one $[\text{Cd}_2(3\text{-bpdb})_2(n\text{-BuO-ip})_2]$. Accordingly, the unit-cell volume is about twice as large as that of **Cd-1'**. Nevertheless, the overlay diagram of the molecules in the two crystal forms (**Cd-1** and **Cd-1'**) indicates that they nearly retain the overall similar molecular conformation at both temperatures.¹² The σ parameter used to quantify the distortion of the octahedral geometry of Cd^{2+} ions was calculated here, and the σ value are 0.49 and 0.47 for **Cd-1** and 0.51 for **Cd-1'**, indicating the slightly less distortion of the polyhedrons in **Cd-1'** (Fig. S2a,d). Taking

a look at the inside view of the both $[\text{Cd}_2(n\text{-BuO-ip})_4]$ dimers, the centroid \cdots centroid distances between phenyl rings in the room-temperature (RT) form are 8.013 and 10.318 Å. But, instead, the corresponding distances in low-temperature form range from 7.904 Å to 10.425 Å, which demonstrated greater diversity (Fig. S2b,e). The largest difference observed is the configuration of the 3-bpdb ligands. The dihedral angle between the pyridine rings is 5.347° in **Cd-1'**, and the corresponding ones are 3.017° and 10.639° in **Cd-1**, suggesting the reduction in symmetry restraint (Fig. S2c,f). Besides, the distance between the backbone of terrace double-layers in **Cd-1** in the low-temperature form is shorter to that observed in the RT form (Fig. S3). In addition, the voids occupy 15.1% of the crystal volume in **Cd-1**, which is smaller than that of **Cd-1'**.

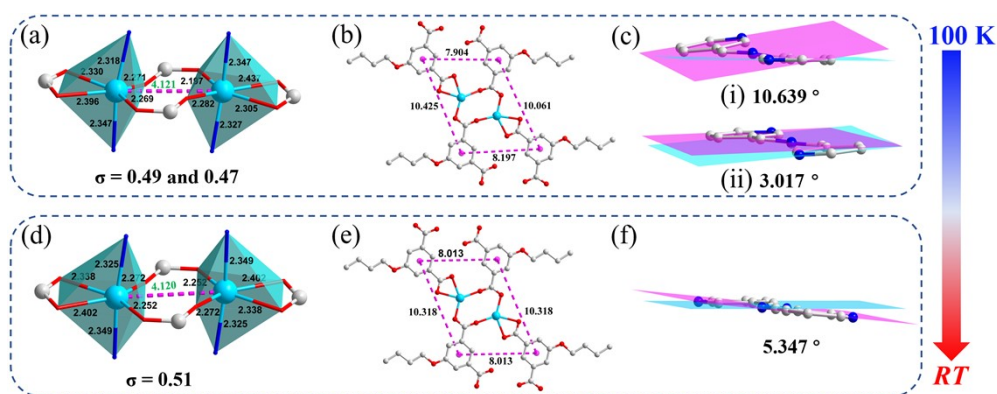


Fig. S2 Diagrams comparing the difference of structural component at RT and 100K. (a) and (d) Polyhedral configuration. (b) and (e) Centroid \cdots centroid distances between phenyl rings of $[\text{Cd}_2(n\text{-BuO-ip})_4]$ dimers. (c) and (f) Dihedral angle between the pyridine rings in 3-bpdb. The units (Å) are omitted for clarity.

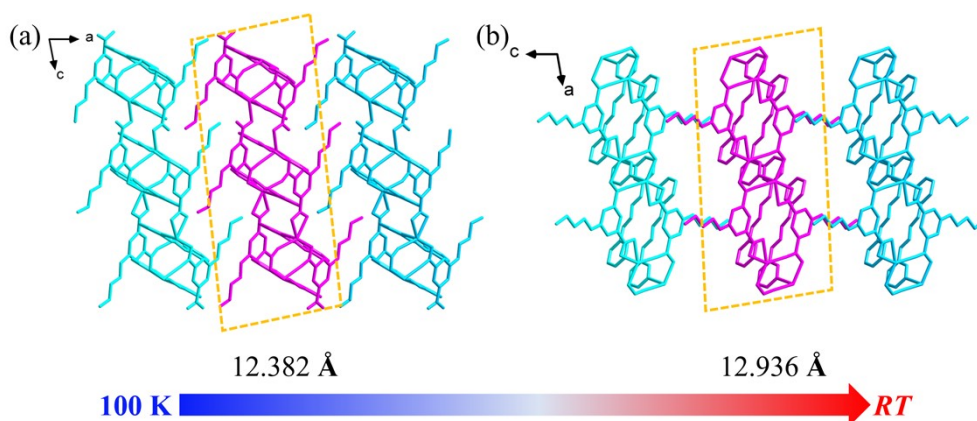


Fig. S3 Distance between the backbone of terrace layers at RT and 100 K.

[Cd(3-bpdb)(*n*-BuO-ip)(H₂O)]_n (**Cd-2**). Structural determination revealed that **Cd-2** exhibits a 2D mono-layered grid-like net and crystallizes in the triclinic space group *P* $\bar{1}$. The asymmetric unit consists of one Cd²⁺ ion, one 3-bpdb ligand, one *n*-BuO-ip²⁻ anion, and one coordinated water (Fig. S4a). Cd1 is in a distorted {CdO₄N₂} octahedral configuration, which is similar to that in **Cd-1'**. However, one bidentate bridging (μ_2 - $\eta^1:\eta^1$) carboxylate oxygen atom in **Cd-1'** is replaced by a terminal coordinated water, which does not involved connecting. As a consequence, the binuclear [Cd₂(COO)₄] unit in **Cd-1'** is transformed to mononuclear [Cd(COO)₂(H₂O)] center. The mononuclear centers are linked by *n*-BuO-ip²⁻ anions with carboxylates by using bidentate chelating (η^2) and monodentate (η^1) modes to form a 1D [Cd(*n*-BuO-ip)(H₂O)]_n chain, with a Cd···Cd distance of 10.387 Å, along the *b*-axis direction (Fig. S4b). Then, 3-bpdb ligands continuously connect the adjacent Cd²⁺ centers to form a 2D mono-layer grid-like structure (Fig. S4c) with **sql** topology (Fig. S4d).

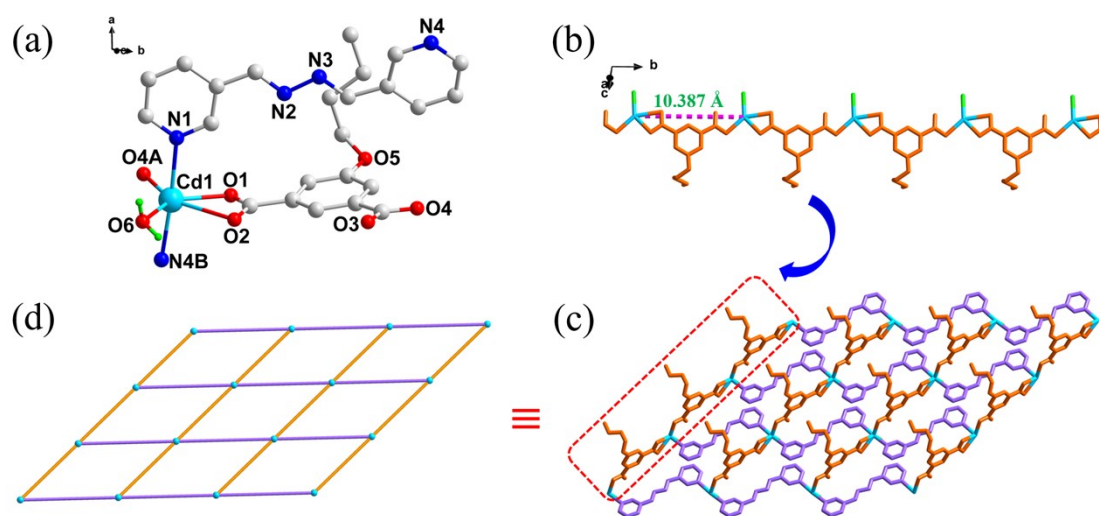


Fig. S4 (a) Coordination environment of Cd²⁺ ion in **Cd-2** (symmetry codes: (A) *x*, *y*-1, *z*; (B) *x*-1, *y*-1, *z*). (b) View of 1D infinite linear [Cd(*n*-BuO-ip)(H₂O)]_n straight chain. (c) 2D monolayer structure. (d) Drawing showing the (4⁴,6²) **sql** topology.

{[Cd₂(3-bpdb)_{2.5}(*n*-BuO-ip)₂(H₂O)]·2H₂O}_n (**Cd-3**). Crystallographic studies showed that **Cd-3** belongs to the *P* $\bar{1}$ space group of the triclinic system, and the asymmetric unit consists of two crystallographically independent Cd²⁺ ions, two *n*-BuO-ip²⁻ anions, two

and a half 3-bpdb ligands, one coordinated water, and two lattice water molecules (Fig. S5a). The crystallographically independent Cd²⁺ ions present different coordinated geometries. Cd1 has a six-coordinate environment consisting of two carboxylates O atoms from two independent *n*-BuO-ip²⁻ ligands, one water O atom, and three N atoms from three 3-bpdb ligands. Cd2 has a five-coordinated triangular bipyramid polyhedron, which is surrounded by three carboxylates O atoms and two axial 3-bpdb N atoms. Similar to that in **Cd-1**, the symmetry-related Cd2 and Cd2A ions in **Cd-3** are bridged by two bidentate bridging ($\mu_2\text{-}\eta^1\text{:}\eta^1$) carboxylate groups, constituting a [Cd₂(COO)₂] SBU with a Cd···Cd distance of 3.935 Å (Fig. S5b). Notably, the alternating mononuclear Cd²⁺ ions and binuclear [Cd₂(COO)₂] SBUs are connected by *n*-BuO-ip²⁻ ligands with the use of $\mu_2\text{-}\kappa^2$ O:O' and $\mu_3\text{-}\kappa^3$ O:O':O'' coordination modes, resulting in a 1D beaded chain with distances between the mono- and bi- metal units of 10.824 and 10.886 Å, respectively (Fig. S5c). The pairwise μ_2 -3bpdb ligands and the binuclear SBUs combine to serve as inclined linear, to produce an **sql** layer (Fig. S5d). The layers are further cross-linked by 3-bpdb at Cd1 atom, thus, a complicated 3D MOF is formed (Fig. S5e). In the 3D framework, each dinuclear (Cd2)₂ unit is six-connected to two (Cd2)₂ units and four mononuclear Cd1 centers, while in turn each Cd1 center is five-connected to two (Cd2)₂ units and three mononuclear Cd1 centers (Fig. S6a). Topological analysis indicated that the 3D framework of **Cd-3** represents a (5,6)-connected binodal new topology with the Schläfli symbol of (4⁵.6⁵)₂(4⁶.6⁸.8) (Fig. S6b). In addition, calculations using PLATON showed that the voids in **Cd-3** occupy 7.9% of the crystal volume (224 Å³ out of the 2835.9 Å³ unit cell volume).

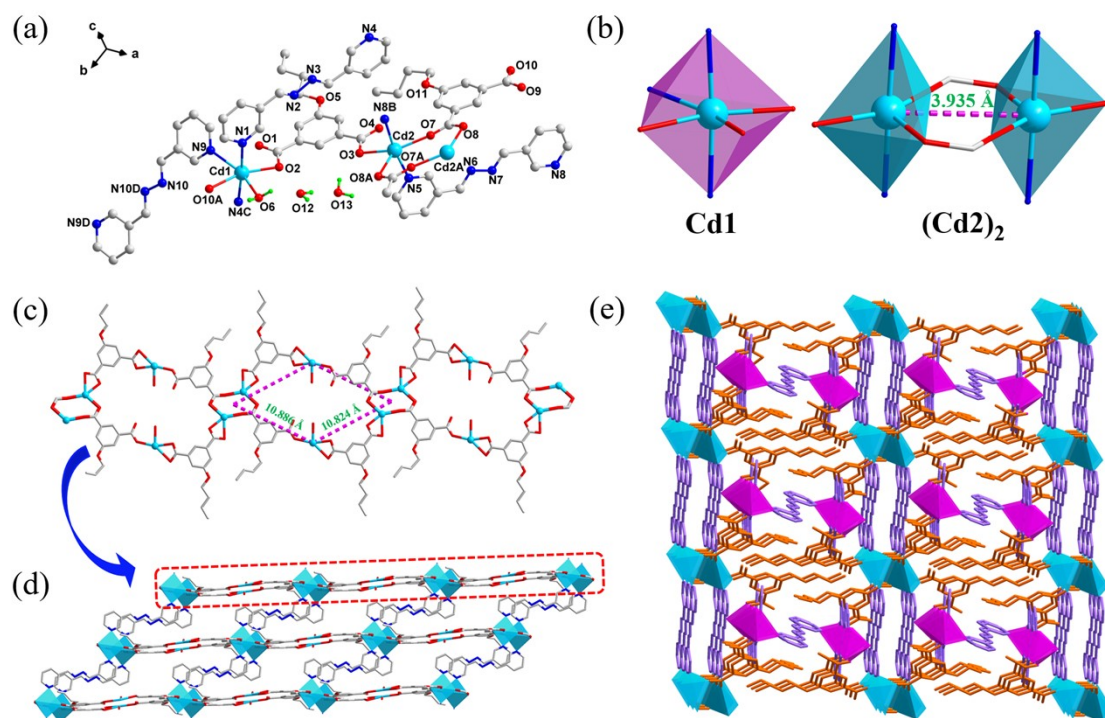


Fig. S5 (a) Coordination environment of Cd^{2+} ion in **Cd-3**. (symmetry codes: (A) $-x+1, -y+1, -z$; (B) $x-1, y, z$; (C) $x, y+1, z$; (D) $-x, -y+3, -z+1$). (b) Polyhedral configuration of Cd1 and Cd2 center. (c) 1D beaded chain composed of $n\text{-BuO-ip}^{2-}$ ligands. (d) A **sq1** layer. (e) 3D framework.

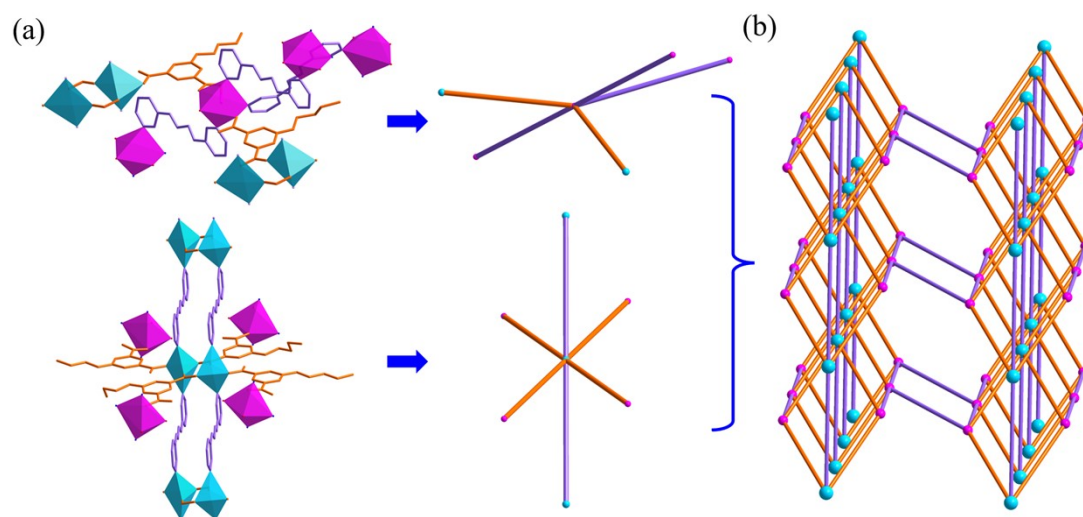


Fig. S6 (a) The 5-connected and 6-connected nodes. (b) Drawing showing the $(4^5.6^5)_2(4^6.6^8.8)$ new topology.

$[\text{Cd}_2(3\text{-bpdb})_2(n\text{-BuO-ip})(n\text{-BuO-Hip})_2(\text{H}_2\text{O})_2]_n$ (**Cd-4**) The crystal structure of **Cd-4** represents a rare example of 1D helical double chains. Different from the other Cd-CPs

reported here, it crystallizes in the monoclinic space group $P2_1/c$, the asymmetric unit consists of two crystallographically independent Cd^{2+} ions, one deprotonated $n\text{-BuO-ip}^{2-}$ anion, two partially deprotonated $n\text{-BuO-Hip}^-$ anions, two 3-bpdb ligands, and two coordinated water molecules (Fig. S7a). Each Cd^{2+} ion is six-coordinated by two $n\text{-BuO-Hip}^-$ O atoms, one $n\text{-BuO-ip}^{2-}$ O atom, one water molecule, and two pyridyl N atoms. As shown in Fig. S7b, the two independent Cd^{2+} ions are held together by one fully deprotonated $n\text{-BuO-ip}^{2-}$ anion with monodentate $\mu_2-(\eta^1)(\eta^1)$ coordination mode, forming a $[\text{Cd}_2(n\text{-BuO-ip})]^{2-}$ dimer. The negative charges of the binuclear core are balanced by the coordination of two partially deprotonated $n\text{-BuO-Hip}^-$ anions with carboxylate groups in bidentate chelating (η^2) mode, continuously forming a $[\text{Cd}_2(n\text{-BuO-ip})(n\text{-BuO-Hip})_2]$ unit. Interestingly, every two 3-bpdb molecules act as μ_2 -bridging linker with the dihedral angles of 38.7° and 59.4° among two pyridyl rings, connecting metal centers to produce a 1D double chain along the a -axis direction (Fig. S7c,d). It is worth noting that the $[\text{Cd}_2(3\text{-bpdb})_2]_n$ motif, featuring a double-helix chain with a long pitch of about 17.13 \AA (Fig. S7e). To date, numerous studies and some landmark reviews have been published on 1D CPs. Linear chains, zigzag architectures, ribbon chains, and ladder chains are the most typical and ubiquitous in 1D CPs. Due to the similarity in biological systems and enantioselective catalysis, the infinite helical structure is the most distinct among the 1D motifs.^{13, 14} In essence, the helical double-chain structure of **Cd-4** is different from the reported ones, such as $\{[\text{Zn}(\text{DPA})(\text{H}_2\text{MDP})]_n \cdot 2(\text{H}_2\text{O})\}_n$ ¹⁵ and $[\text{Mn}_2(\text{ip})_2(\text{bpy})_2]_n$ ¹⁶ for the two helical chains in **Cd-4** are locked by the monodentate bridging $n\text{-BuO-ip}^{2-}$ anions. As far as we know, this unique structural motif in 1D CPs has never been reported before, and will enrich the field of 1D chain polymers. Topologically, each Cd^{2+} atom can be regarded as a 3-connected node and the structure of **Cd-4** can be simplified as a uninodal 3-c net with the Schlafli symbol of $(4^2.6)$ (Fig. S7f).

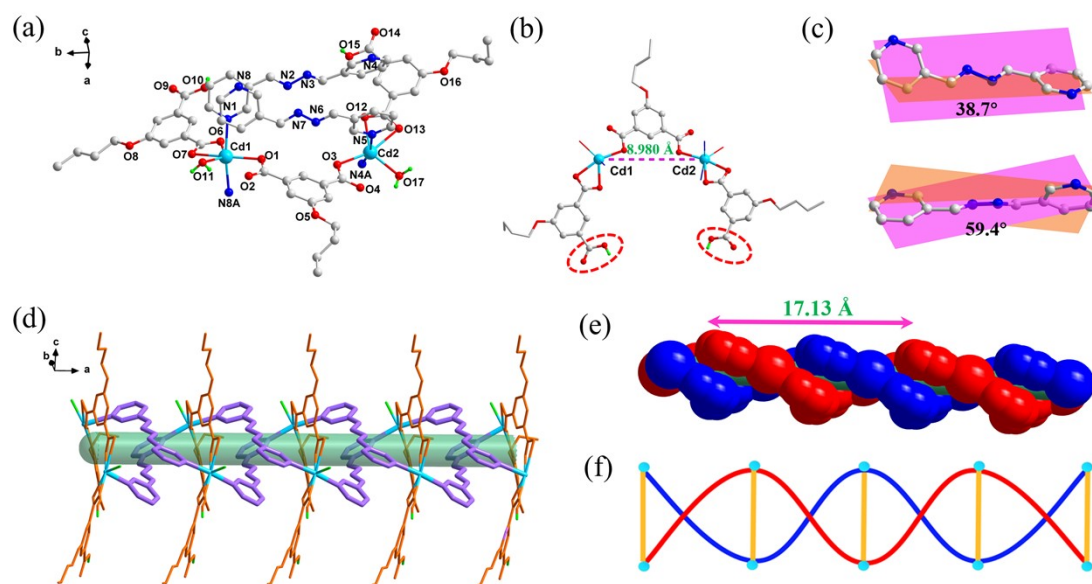


Fig. S7 (a) Coordination environment of Cd^{2+} ions in **Cd-4**. (symmetry codes: (A) $x+1$, y , z). (b) Connectivity and geometry of $[\text{Cd}_2(n\text{-BuO-ip})(n\text{-BuO-Hip})_2]$ dimer. The partially deprotonated $n\text{-BuO-Hip}^-$ anions are highlighted. (c) Configuration and dihedral angles of among the pyridyl rings in 3-bpdb ligands. (d) 1D double chain structure of **Cd-4**. (e) Double-helix chains. (f) Simplified view of the 1D infinite chain structure.

$\{[\text{Cd}(3\text{-bpdb})_{0.5}(n\text{-BuO-ip})(\text{DMF})(\text{H}_2\text{O})] \cdot \text{H}_2\text{O}\}_n$ (**Cd-5**). Structural determination revealed that the stoichiometric ratio of metal to the bipyridyl ligand and carboxylic acid is 1:0.5:1. Besides, the asymmetric unit includes one coordinated DMF, one coordinated water, and one lattice water molecule. As shown in Fig. S8a, each Cd^{2+} ion has a distorted $\{\text{CdO}_5\text{N}\}$ octahedral geometry, and the equatorial plane is built by three carboxylate O atoms from two independent $n\text{-BuO-ip}^{2-}$ and a pyridyl N atom. One DMF oxygen and one water O atoms occupy the axial positions. As expected, the $\text{Cd}-\text{N}_{3\text{-bpdb}}$ bond length of 2.32 Å is in the normal range, however, the bond lengths of $\text{Cd}-\text{O}_{\text{carboxylate}} (\eta^2\text{-COO}^{2-})$ (2.37 and 2.44 Å) are longer than those of $\text{Cd}-\text{O}_{\text{carboxylate}} (\eta^1\text{-COO}^{2-})$ bond (2.23 Å) and $\text{Cd}-\text{O}_{\text{water}}$ bond (2.28 Å) lengths, showing weak interaction of $\text{Cd}-\text{O} (\eta^2\text{-COO}^{2-})$. In **Cd-5**, the $n\text{-BuO-ip}^{2-}$ ligands link the adjacent $[\text{Cd}(\text{H}_2\text{O})(\text{DMF})]^{2+}$ centers with carboxylate groups function as chelated bidentate (η^2) and monodentate (η^1) bridges, generating a 1D $[\text{Cd}(n\text{-BuO-ip})(\text{H}_2\text{O})(\text{DMF})]_n$ linear

chain along the *b*-axis. Further, the two crystallographically equivalent neighboring chains are connected by 3-bpdb ligands to form a 1D ladder-like double-chain structure with Cd \cdots Cd separations of 10.296 and 13.218 Å, respectively (Fig. S8b,c). Notably, the two pyridyl rings of 3-bpdb are coplanar in **Cd-5**, different to those of the Cd-CPs.

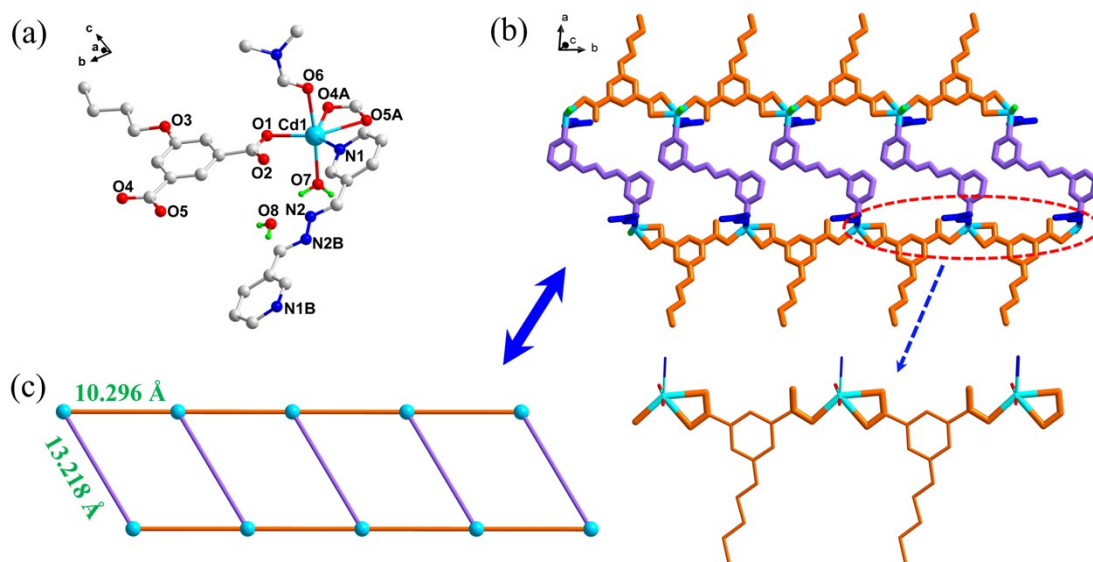


Fig. S8 (a) Coordination environment of Cd $^{2+}$ ion in **Cd-5** (symmetry codes: (A) $x, y-1, z$; (B) $-x, -y+1, -z+1$). (b) 1D ladder-like double chains along the *b*-axis.

$\{[\text{Cd}_2(3\text{-bpdb})(n\text{-BuO-ip})_2(\text{H}_2\text{O})_4]\cdot\text{H}_2\text{O}\}_n$ (**Cd-6**). The double-chain ladder-like structure of **Cd-6** is similar to that of **Cd-5**, with the nodes and rungs and rails in a ratio of 1:0.5:1. The asymmetric unit consists of two crystallographically independent Cd $^{2+}$ ion, two *n*-BuO-ip $^{2-}$ anions, one 3-bpdb ligand, and four coordinated water molecules, and one lattice water molecule (Fig. S9a). Cd1 is six-coordinated in a distorted {CdO5N} octahedral geometry, whereas Cd2 is seven-coordinated in a distorted {CdO6N} pentagonal bipyramid geometry. The main reason for the difference lies in the coordination mode of carboxylate groups, as shown in Fig. S9b (zoomed image). In **Cd-6**, the distance of the rung is 14.605 Å, which is slightly longer than that in **Cd-5**, indicating the non-coplanar of 3-bpdb ligands (the dihedral angle between the pyridine rings is 7.245°). While the distance of the rail in **Cd-6** is 10.012, which is slightly shorter than the corresponding one in **Cd-5**, implying the coordination differences of *n*-BuO-ip $^{2-}$ ligands (Fig. S9c). Indeed, each linear chain of the ladder in **Cd-6** is formed by the alternate linking of $\mu_2-(\eta^2)(\eta^2)\text{-}n\text{-BuO-ip}^{2-}$ and $\mu_2-(\eta^1)(\eta^2)\text{-}n\text{-BuO-ip}^{2-}$ of Cd $^{2+}$

ions, different to the unitary linking of $\mu_2-(\eta^1)(\eta^2)-n\text{-BuO-ip}^{2-}$ in **Cd-5**.

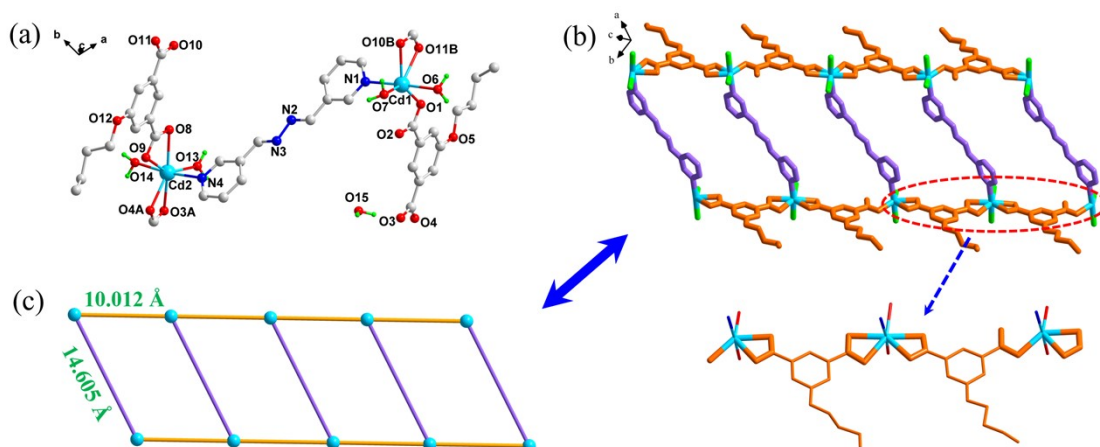


Fig. S9 (a) Coordination environment of Cd²⁺ ion in **Cd-6** (symmetry codes: (A) $-x+1, -y+1, -z$; (B) $-x+2, -y+2, -z+1$). (b) Polyhedral configuration of Cd1 and Cd2 center. (c) Terraced-chain 1D coordination polymer structure.

$[\text{Cd}(3\text{-bpdb})_{0.5}(n\text{-BuO-ip})(\text{H}_2\text{O})]_n$ (**Cd-7**). Structure analysis showed that **Cd-7** features a 2D mono-layered structure with 3,4-connected binodal V_2O_5 -type network, which is obviously different with the (3,5)-connected double-layered terrace structure of **Cd-1'** and the mono-layered grid-like structure of **Cd-2**. The asymmetric unit of **Cd-7** comprises one $[\text{Cd}(3\text{-bpdb})_{0.5}(n\text{-BuO-ip})(\text{H}_2\text{O})]$ (Fig. S10a). Each Cd²⁺ center is seven coordinated, having a pentagonal bipyramidal geometry where its coordination environment is satisfied by one N atom of 3-bpdb ligand and six O atoms, among five are coming from three anion $n\text{-BuO-ip}^{2-}$ ligands and the sixth belongs to water. The $n\text{-BuO-ip}^{2-}$ anion adopts a μ_3 -coordination fashion with one carboxylate group adopting a bidentate chelating (η^2) mode, while the other shows a chelating-bridging ($\eta^2:\eta^1$) tridentate mode. The $\mu_3-(\eta^2)(\eta^2:\eta^1)-n\text{-BuO-ip}^{2-}$ ligands bridge Cd²⁺ ions to form a 1D double chain with Cd \cdots Cd distances of 3.958 and 10.106 Å, respectively (Fig. S10b). The 3-bpdb ligand adopts 2-bridging modes by sharing Cd²⁺ centers from the 1D $[\text{Cd}(n\text{-BuO-ip})]_n$ double chains to generate a 2D layer (Fig. S10c). Topologically, **Cd-7** can be simplified as a 3,4-connected V_2O_5 -type network with the Schlafli symbol of $(4^2.6)(4^2.6^3.8)$, in which $n\text{-BuO-ip}^{2-}$ can be regarded as the 3-connected node to bridge three Cd²⁺ ions and each Cd²⁺ as a 4-connected node by linking to three $n\text{-BuO-ip}^{2-}$ ions and one Cd²⁺ via 3-bpdb (Fig. S10d).

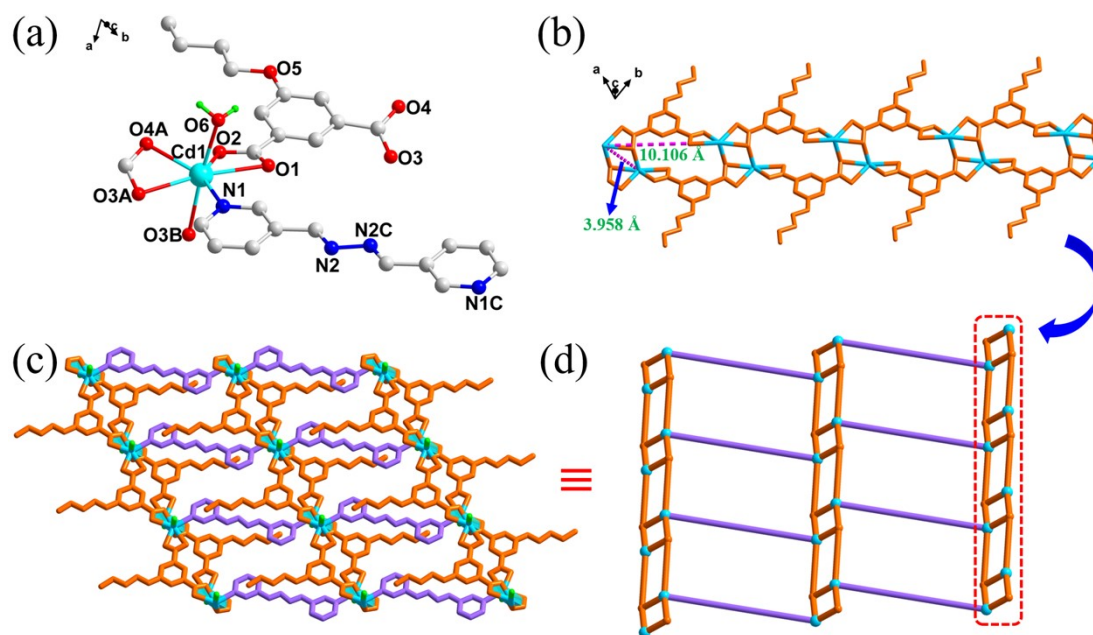


Fig. S10 (a) Coordination environment of Cd²⁺ ion in Cd-7 (symmetry codes: (A) $x+1, y-1, z$; (B) $-x+1, -y+1, -z+1$; (C) $-x+1, -y+1, -z+2$). (b) 1D double chain. (c) 2D layer structure. (d) Drawing showing the $(4^2.6)(4^2.6^3.8)$ topology.

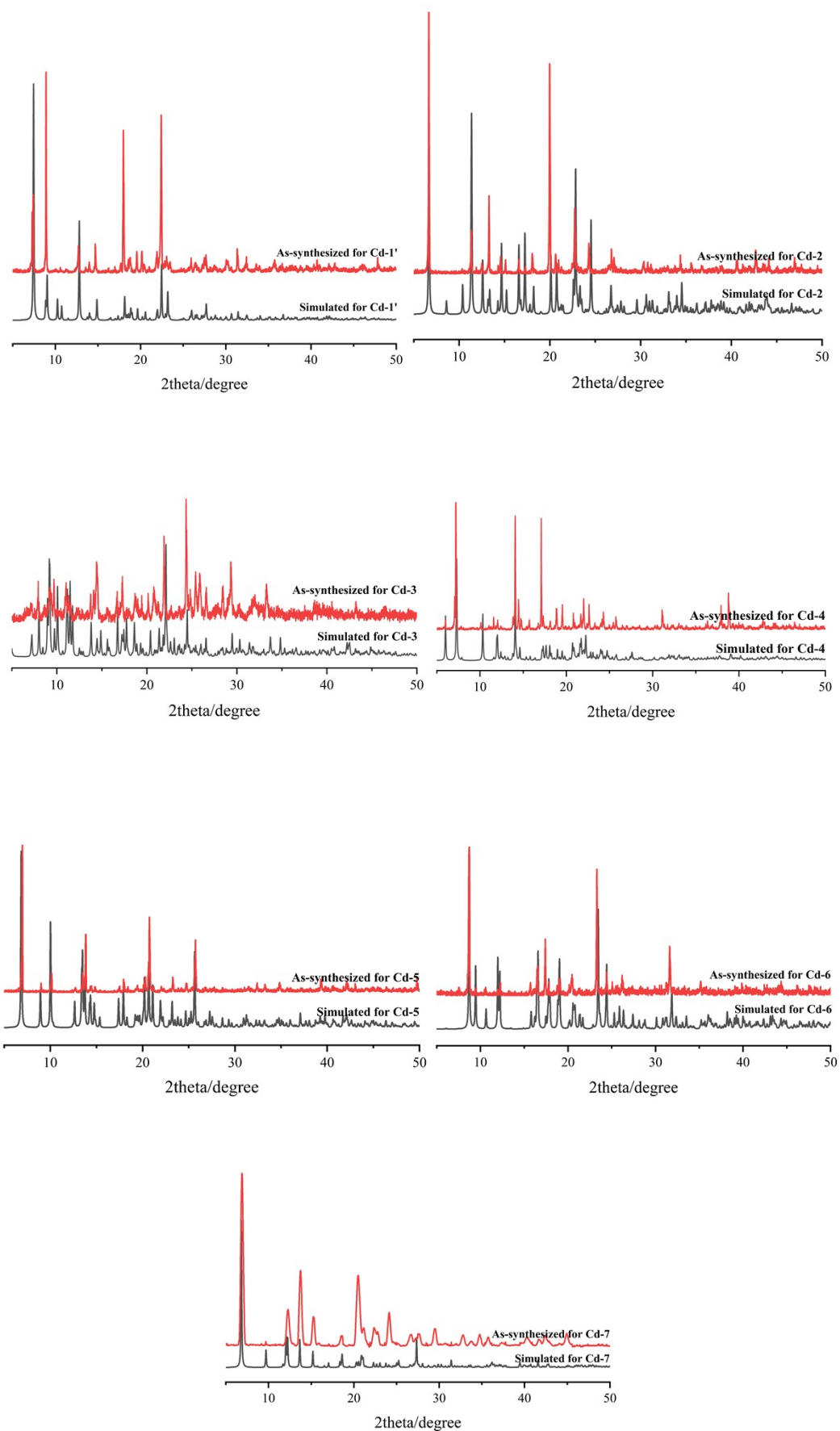


Fig. S11. Simulated and as-synthesized PXRD patterns for Cd-CPs.

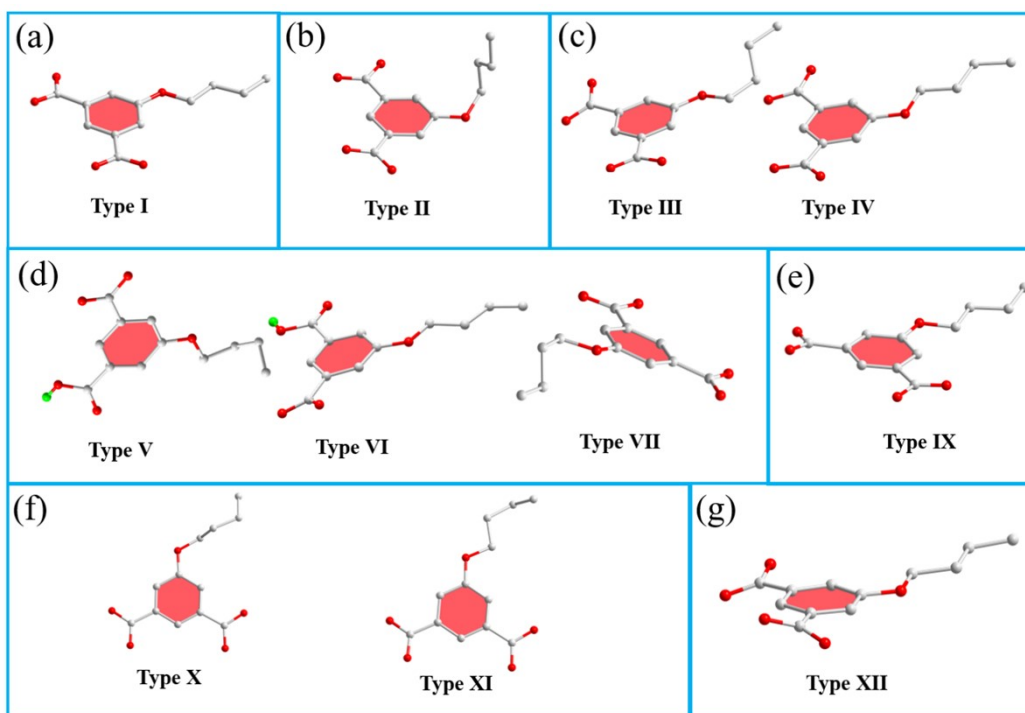


Fig. S12 Twisting of the alkoxy chain in the different conformations of (a) **Cd-1'** (b) **Cd-2** (c) **Cd-3** (d) **Cd-4** (e) **Cd-5** (f) **Cd-6** (g) **Cd-7**.

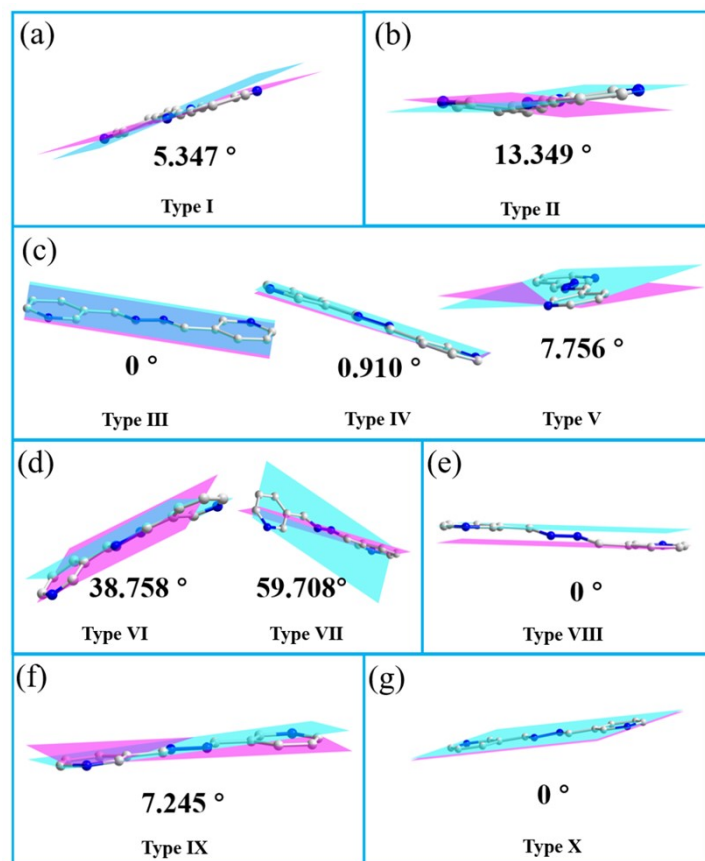


Fig. S13 Dihedral angles between pyridine rings in 3-bpdb of (a) **Cd-1'** (b) **Cd-2** (c) **Cd-3** (d) **Cd-4** (e) **Cd-5** (f) **Cd-6** (g) **Cd-7**.

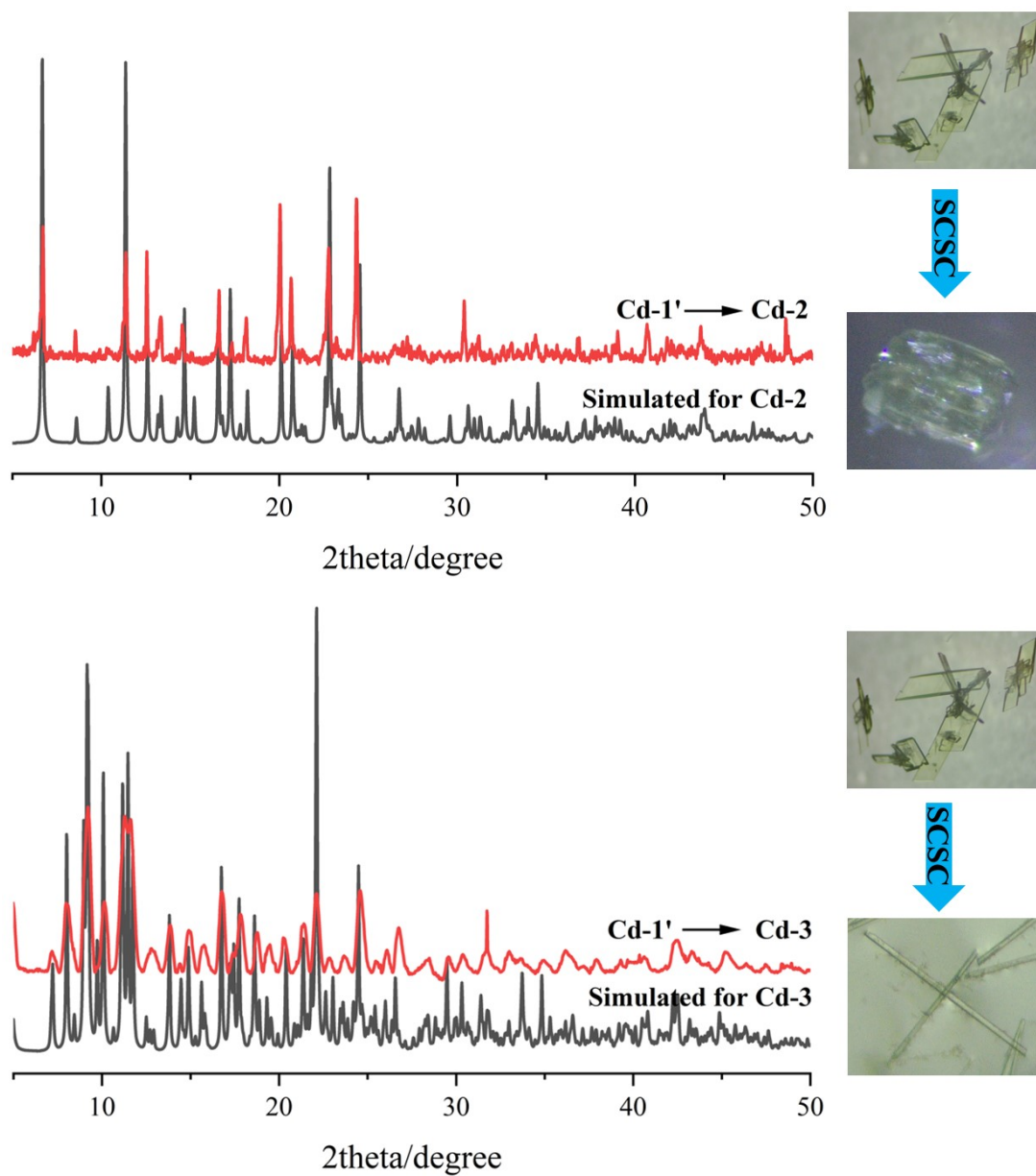


Fig. S14 SCSC transformation PXRD patterns for Cd-1' to Cd-2 and Cd-3.

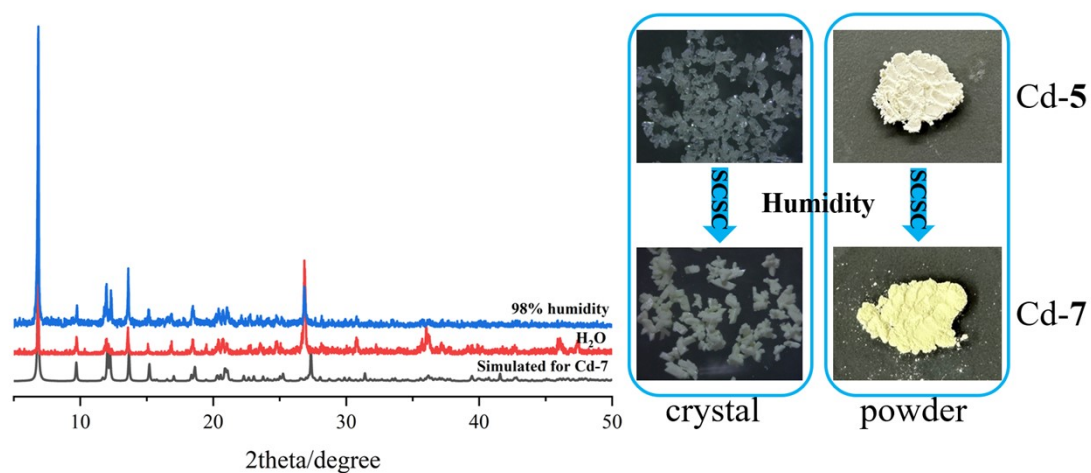


Fig. S15 SCSC transformation PXRd patterns for Cd-5 to Cd-7.

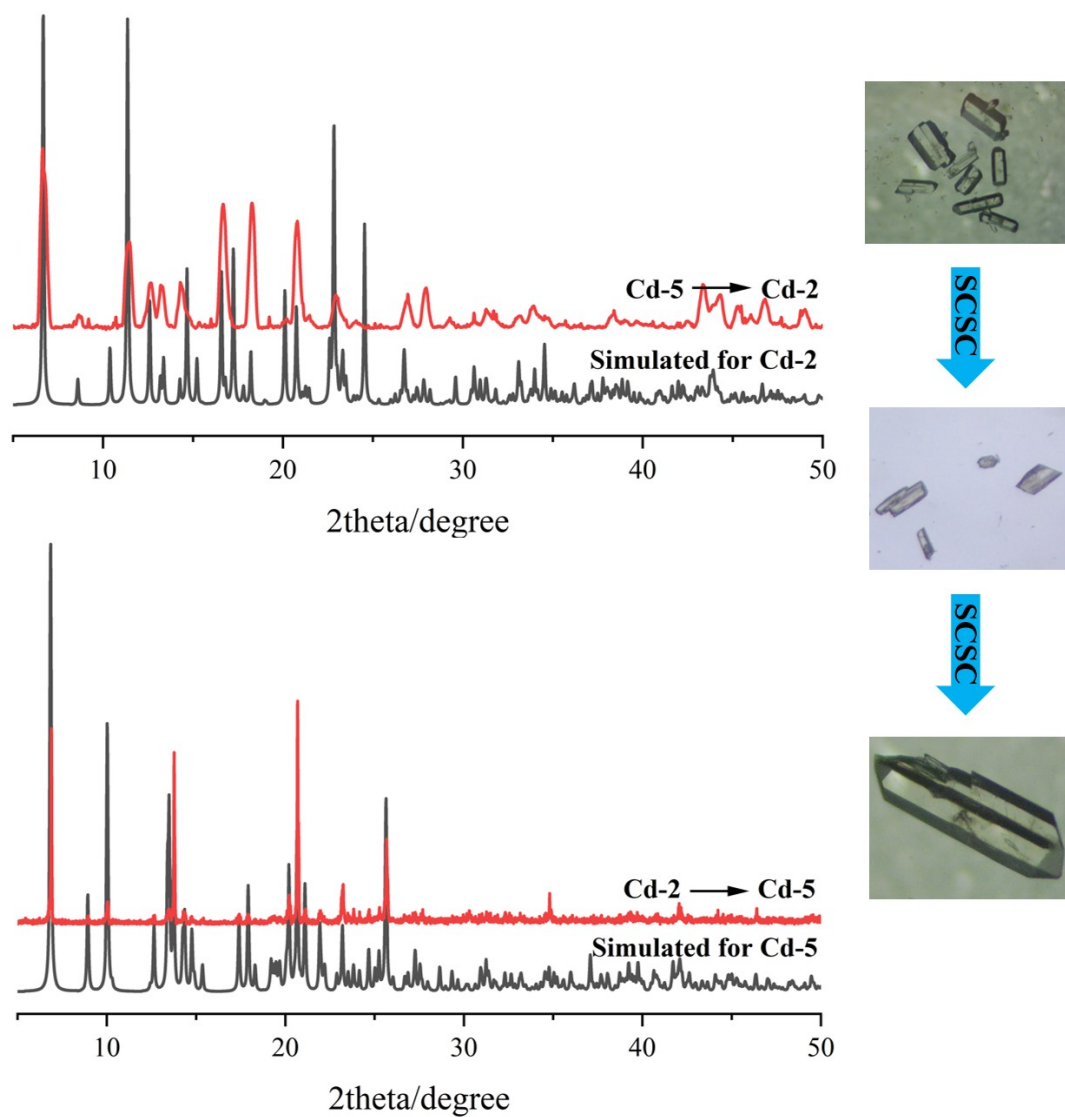


Fig. S16 SCSC transformation PXRd patterns for between Cd-5 and Cd-2

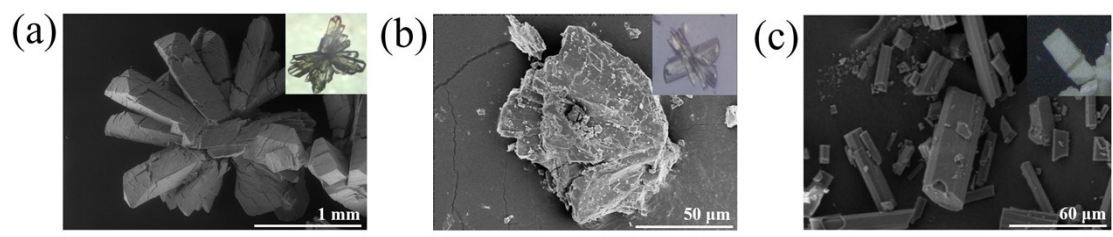


Fig. S17 SEM of (a) Cd-5, (b) Cd-6, (c) Cd-7. Insert: photograph.

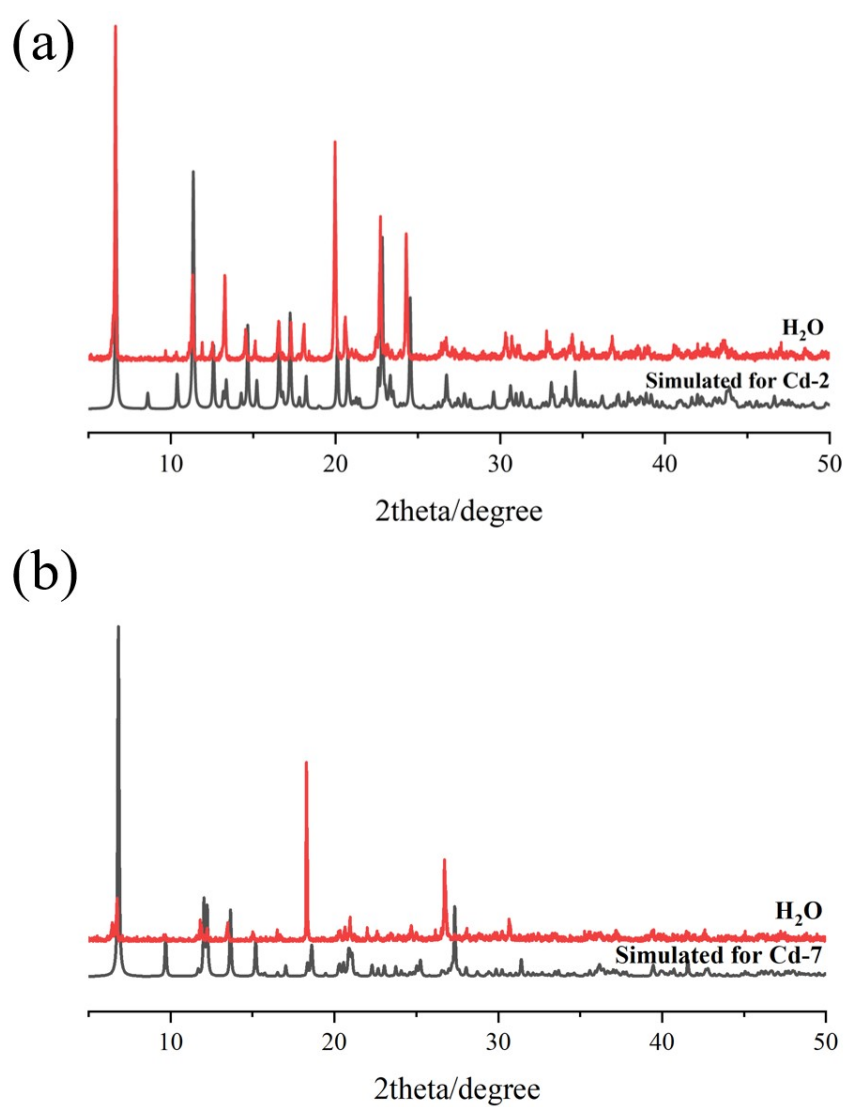


Fig. S18 PXRD patterns of (a) Cd-2 and (b) Cd-7 immersed in aqueous solutions for 35 days.

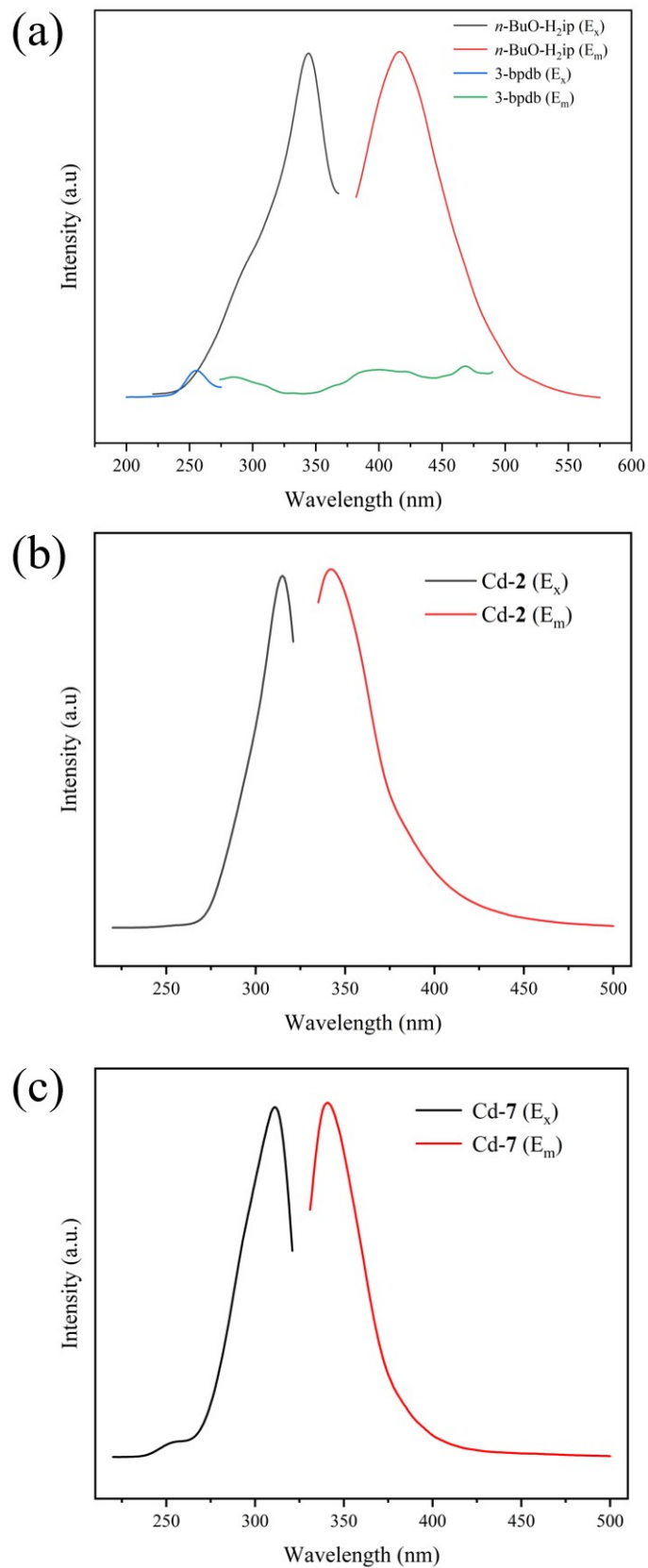


Fig. S19 (a) Solid-state emission and excitation spectra of *n*-BuO-H₂ip and 3-bpdb. Emission and excitation spectra in aqueous solution of (b) **Cd-2** and (c) **Cd-7**.

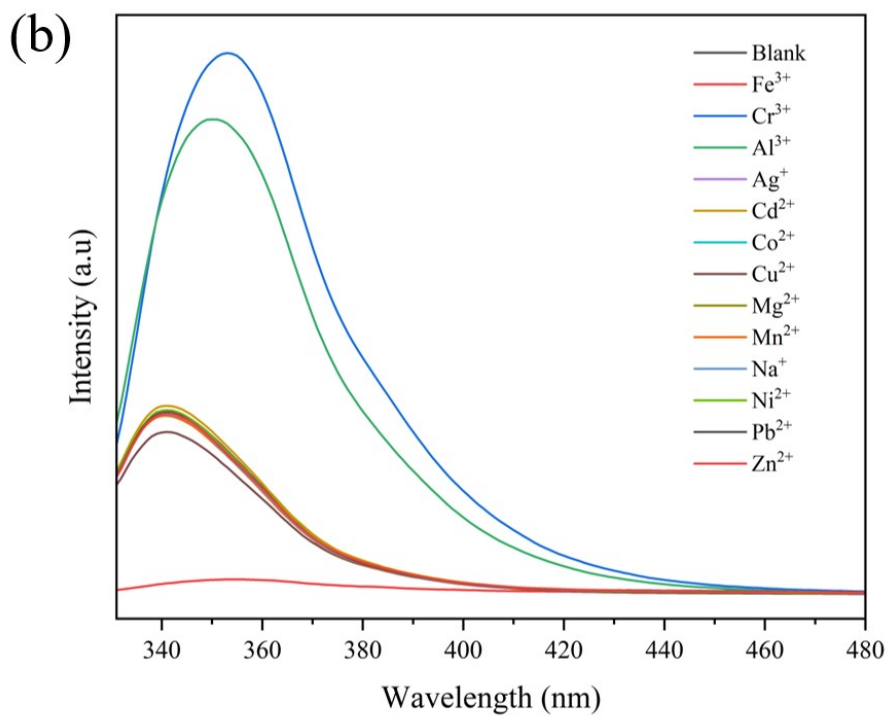
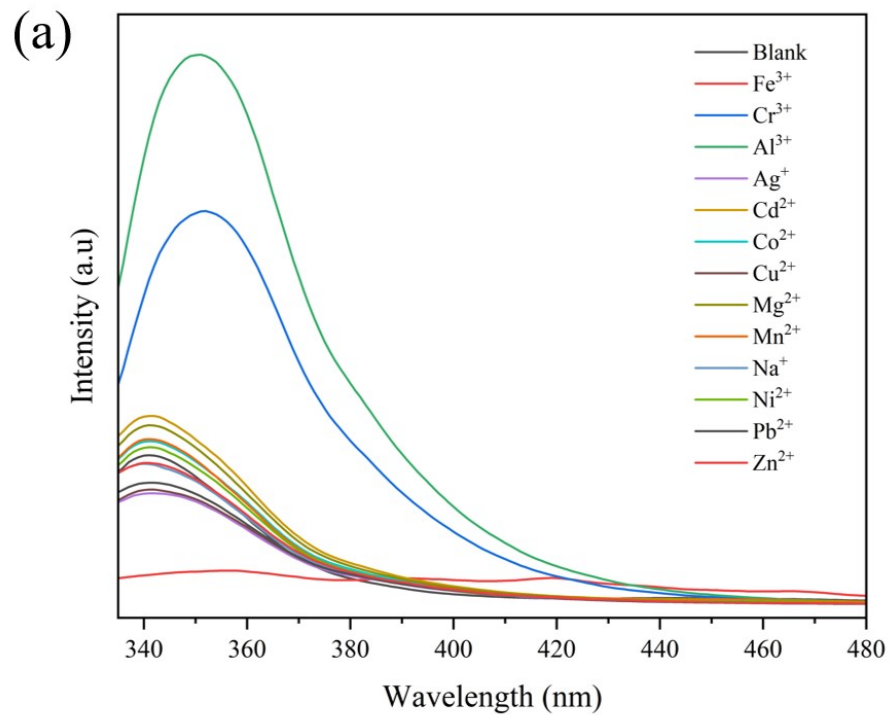


Fig. S20 Emission spectra of (a) **Cd-2** and (c) **Cd-7** in different cations.

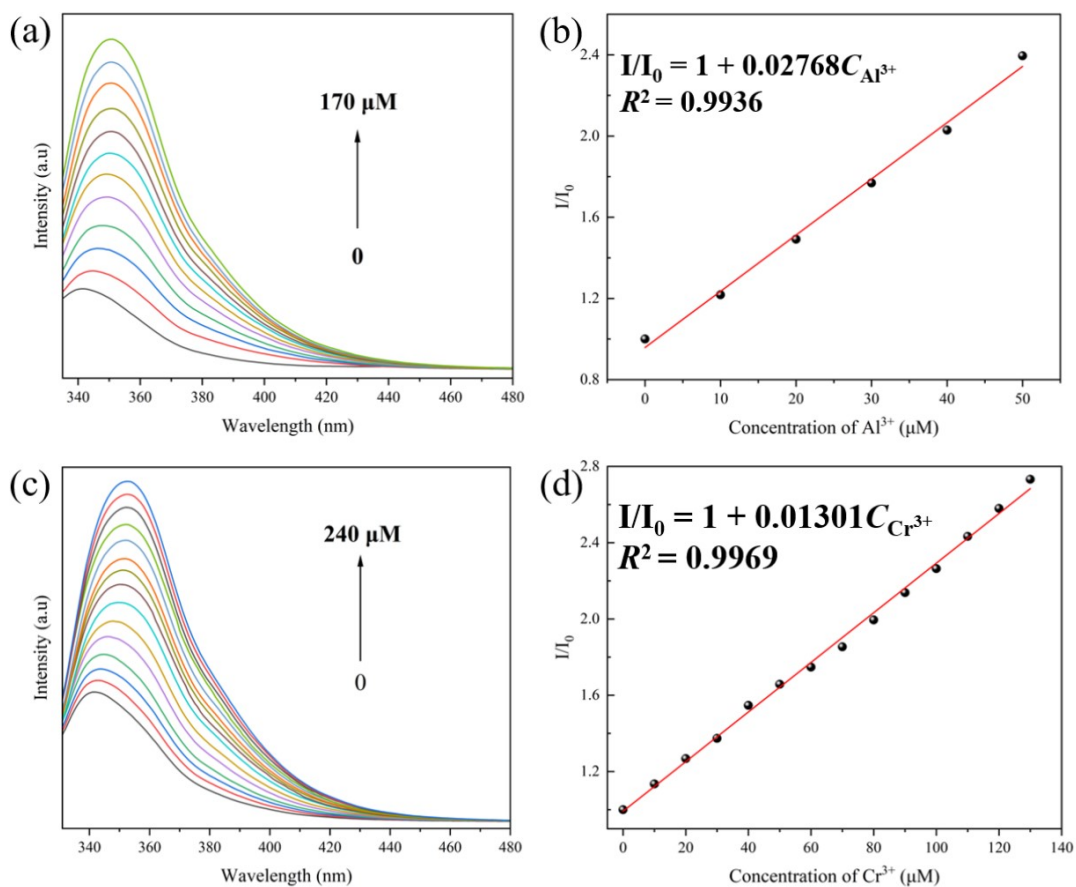


Fig. S21 Emission spectra of Cd-2 immersed in aqueous solutions with (a) Al³⁺ and (c) Cr³⁺ at different concentrations. Fitting curve of I/I_0 vs (b) Al³⁺ and (d) Cr³⁺ concentration ($\lambda_{ex} = 311$ nm).

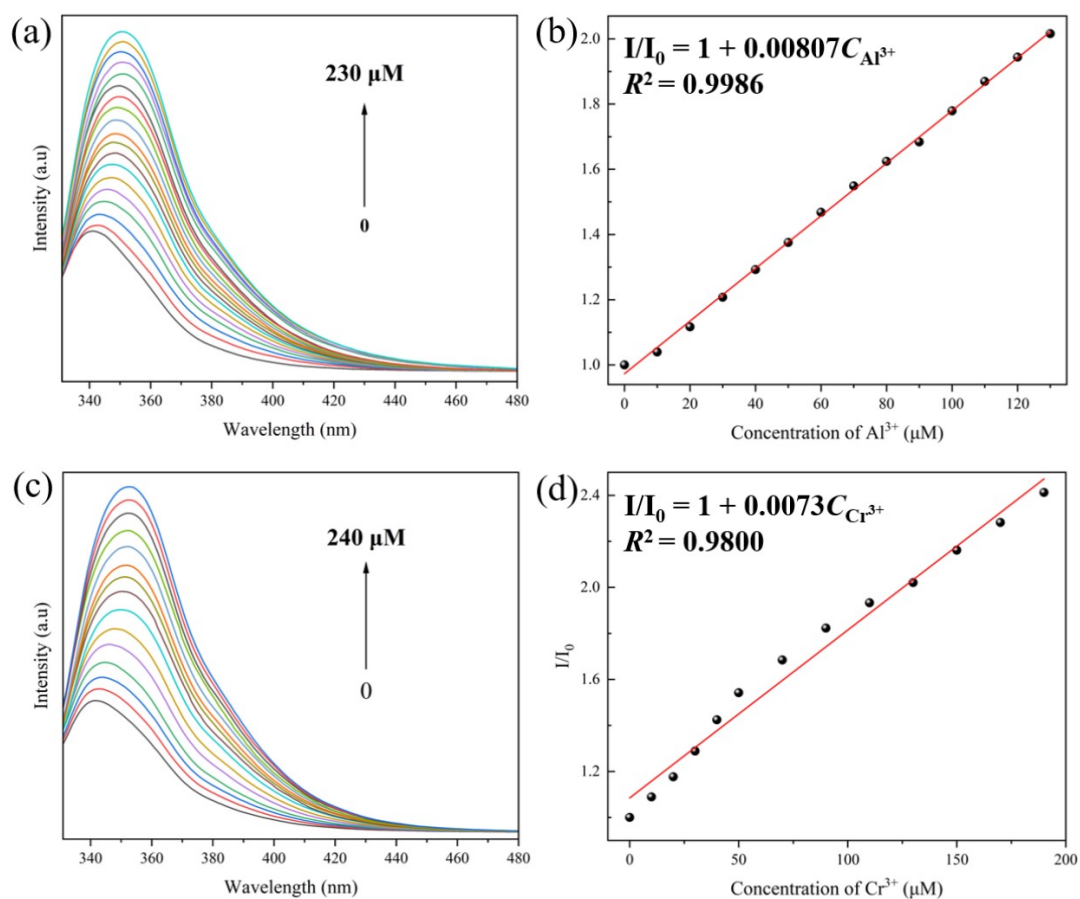


Fig. S22 Emission spectra of Cd-7 immersed in aqueous solutions with (a) Al³⁺ and (c) Cr³⁺ at different concentrations. Fitting curve of I/I_0 vs (b) Al³⁺ and (d) Cr³⁺ concentration ($\lambda_{ex} = 311$ nm).

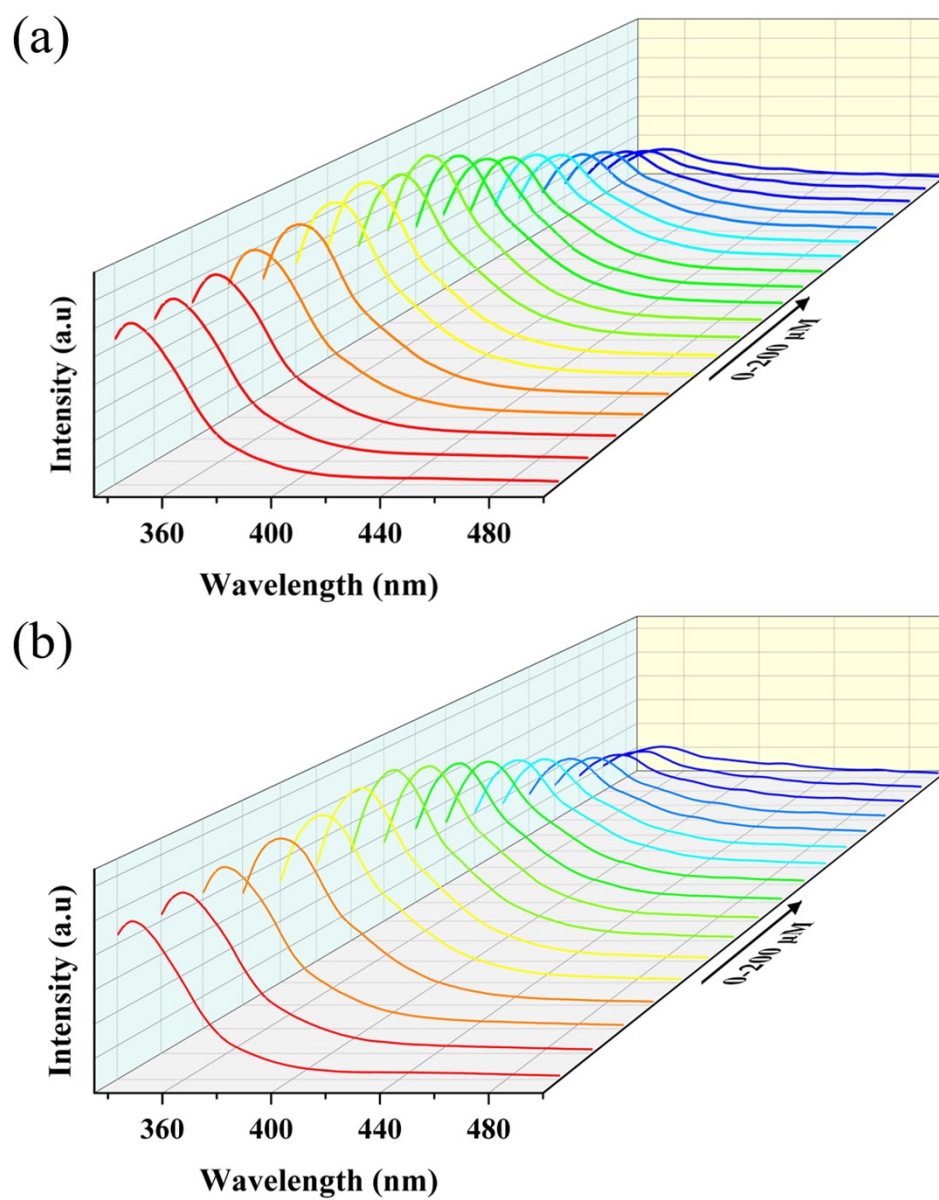


Fig. S23 Fluorescence emissions of Cd-2 to Fe³⁺ within (a) 2 cycles and (b) 3 cycles.

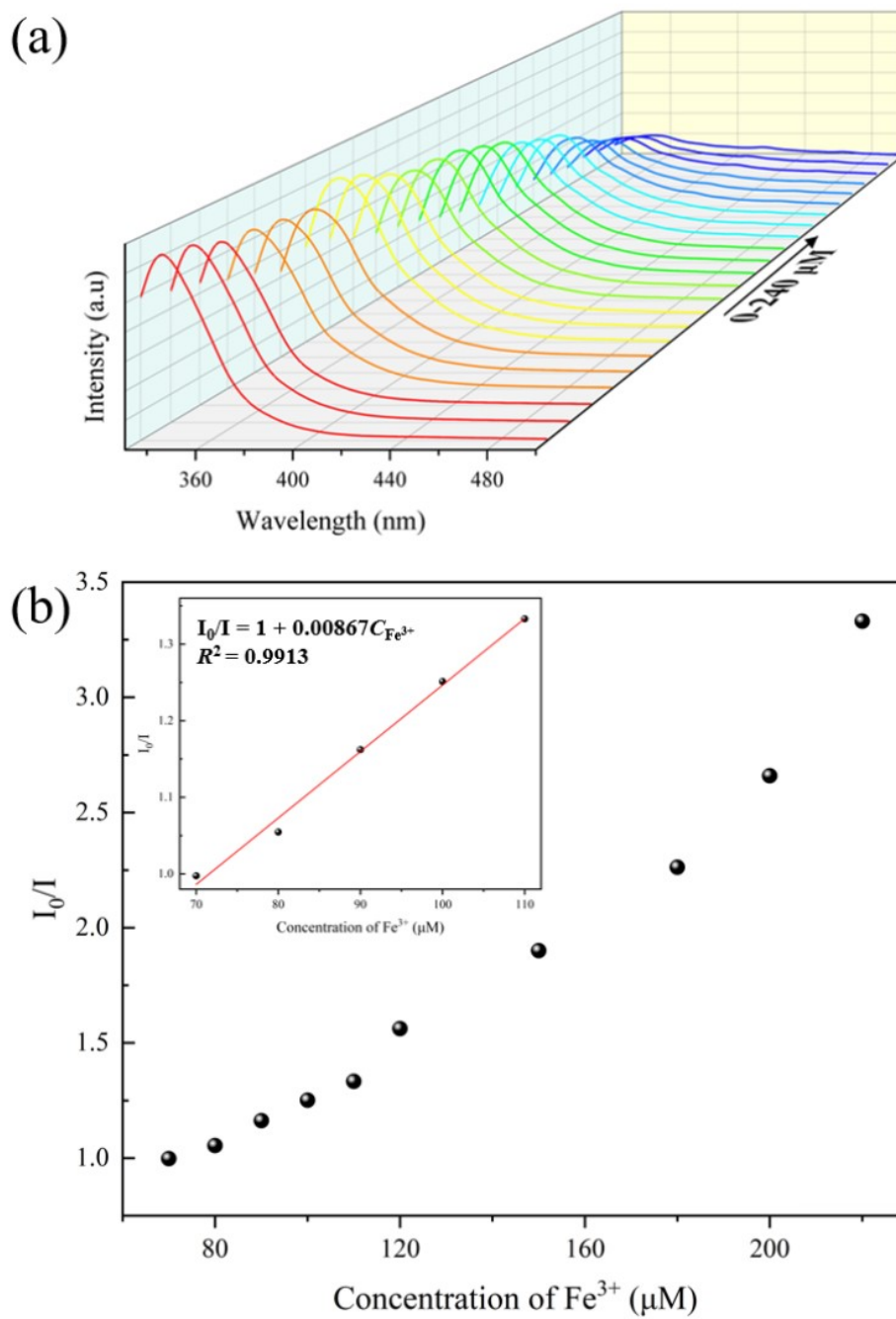


Fig. S24 (a) Emission spectra of Cd-7 immersed in aqueous solutions with Fe^{3+} at different concentrations. (b) Fitting curve of I/I_0 vs Fe^{3+} concentration ($\lambda_{\text{ex}} = 311 \text{ nm}$)

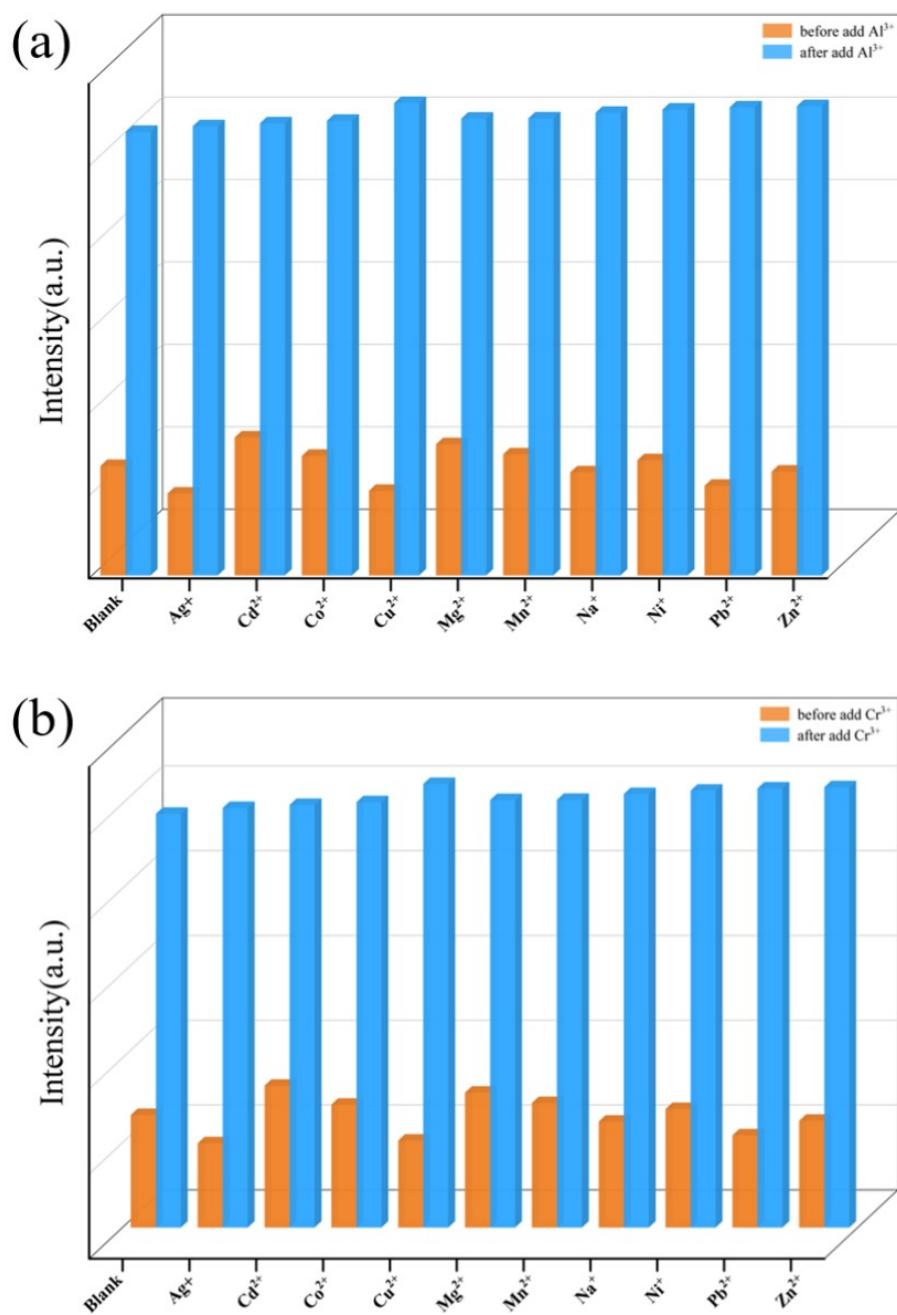


Fig. S25 (a) Selective detection of (a) Cr^{3+} and (b) Al^{3+} by Cd-2 in the presence of other cations in the aqueous medium.

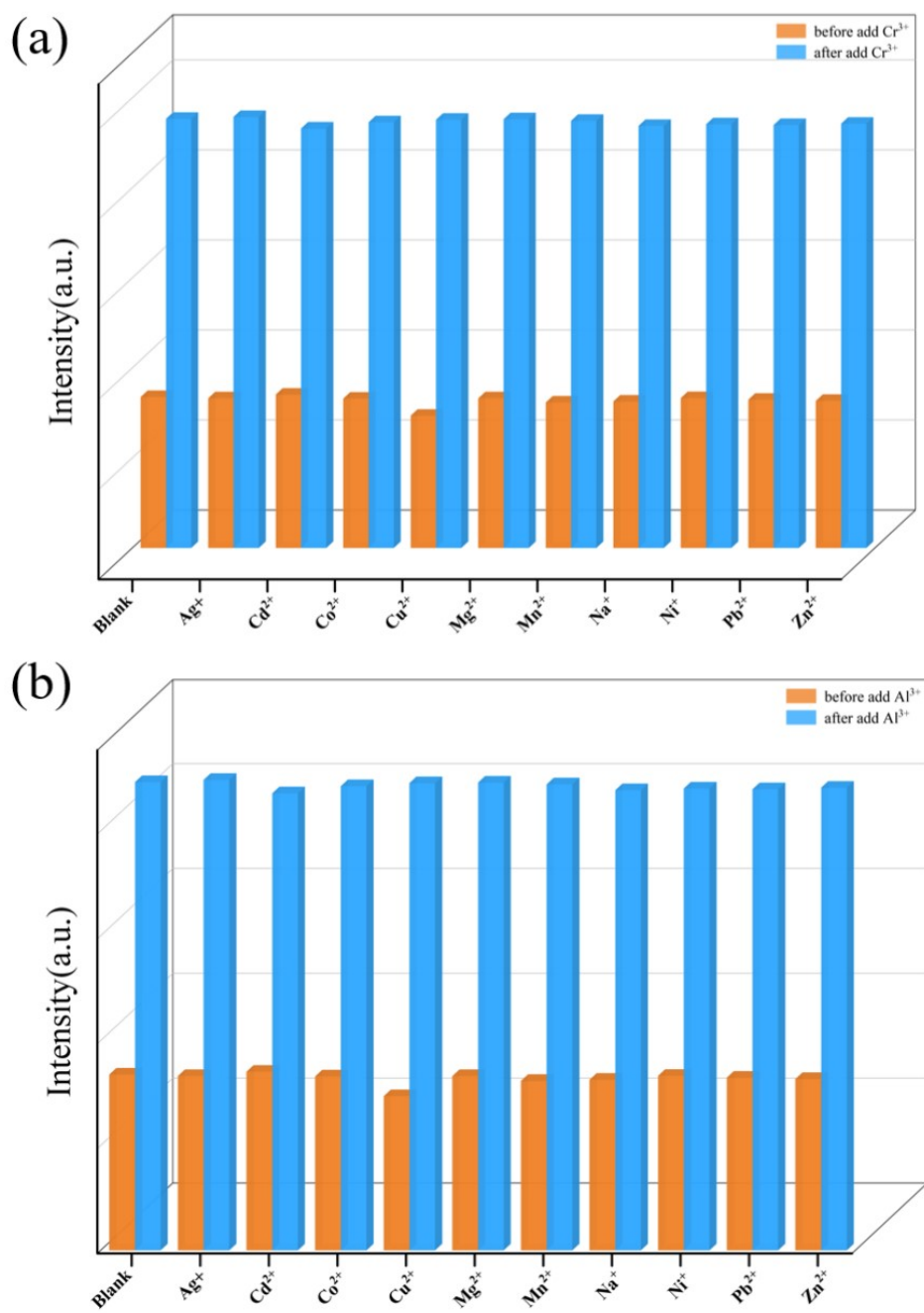


Fig. S26 (a) Selective detection of (a) Cr³⁺ and (b) Al³⁺ by Cd-7 in the presence of other cations in the aqueous medium.

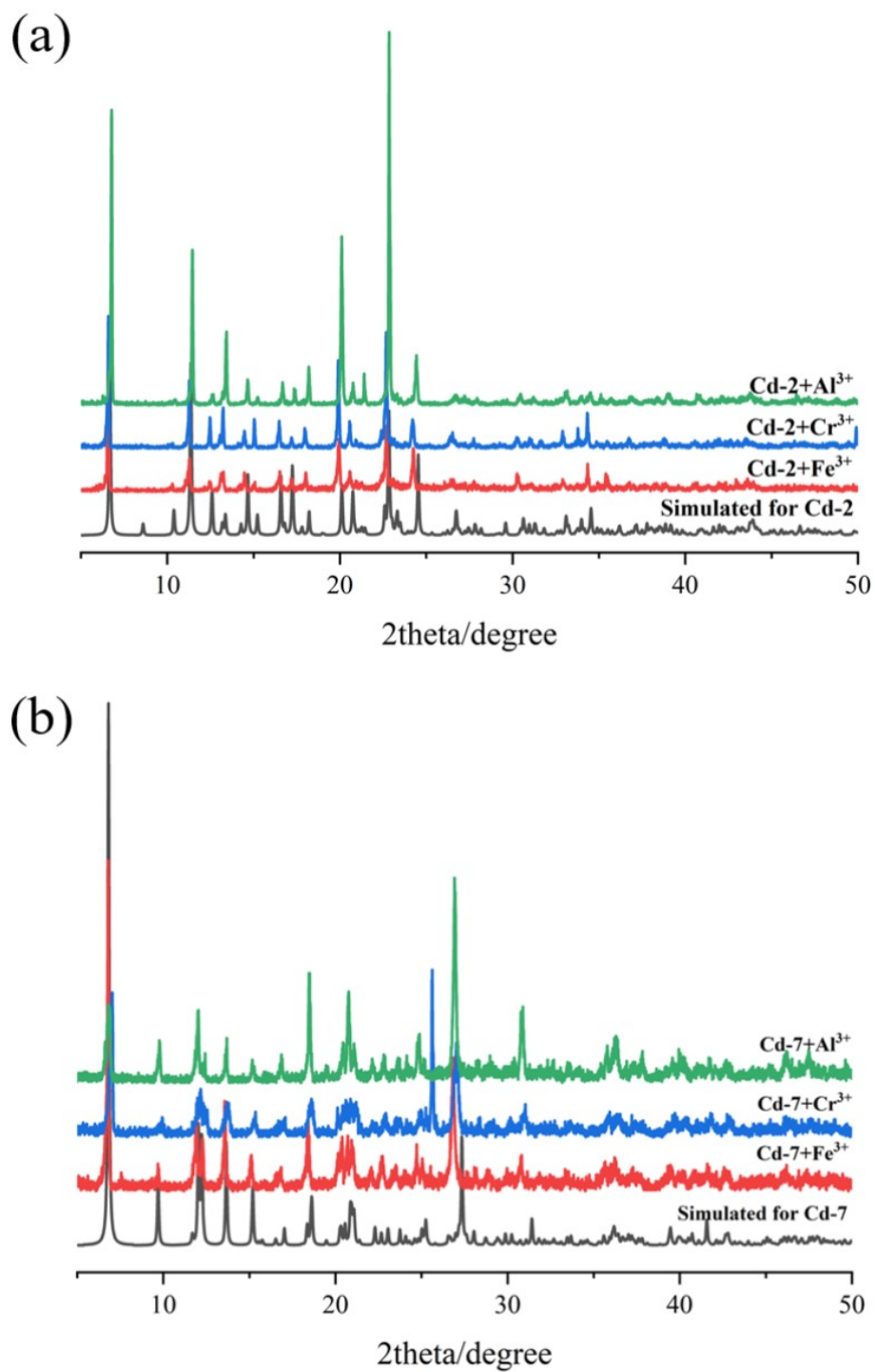


Fig. S27 PXR D patterns of (a) Cd-2 and (b) Cd-7 after sensing Al³⁺, Cr³⁺, and Fe³⁺.

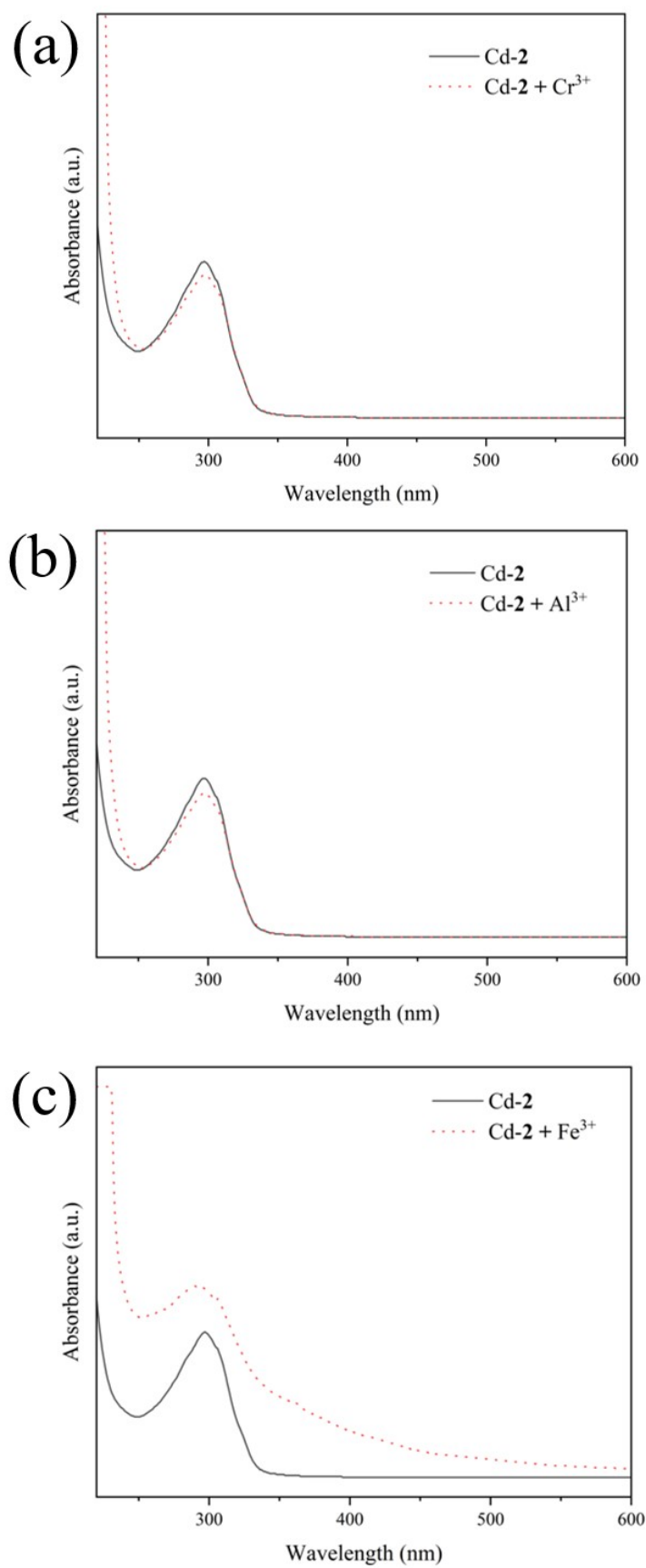


Fig. S28 UV-vis absorption spectrum of **Cd-2** and with the addition of (a) Cr³⁺, (b) Al³⁺ and (c) Fe³⁺.

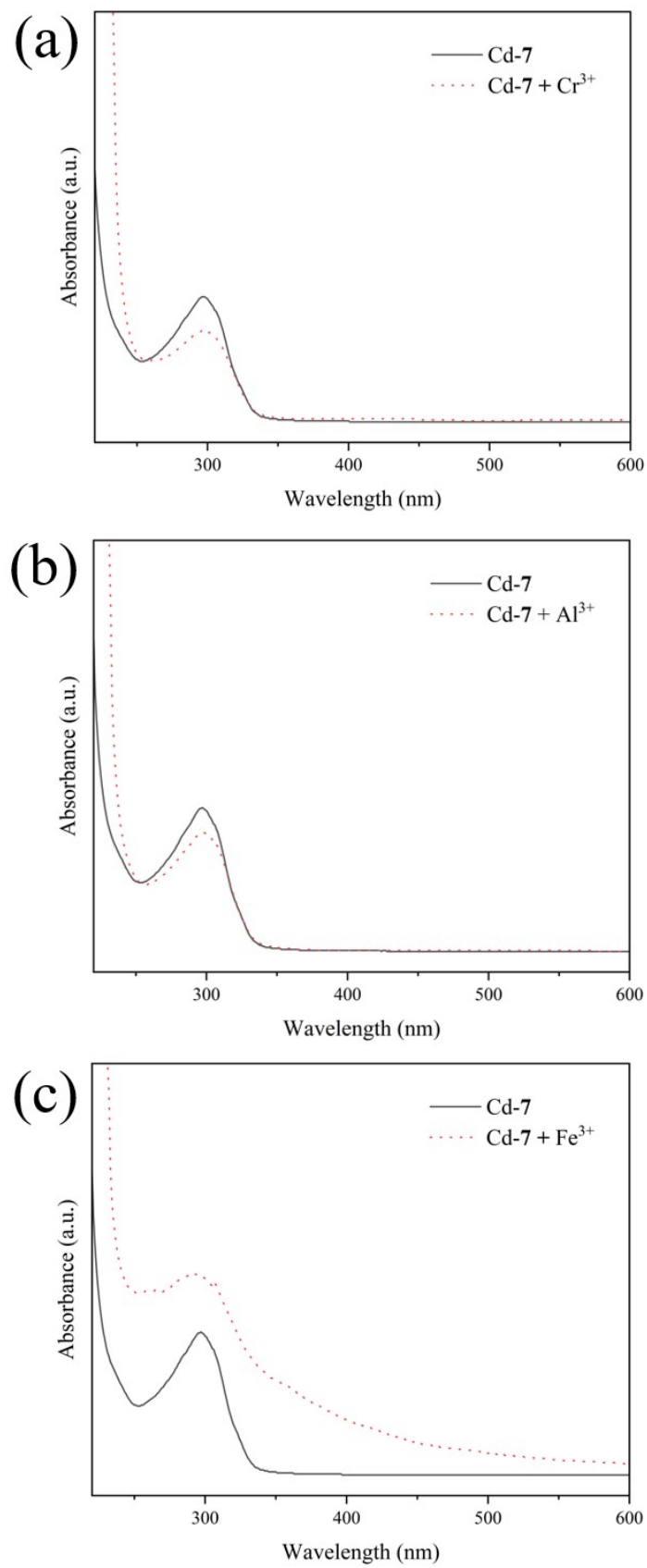


Fig. S29 UV-vis absorption spectrum of **Cd-7** and with the addition of (a) Cr³⁺, (b) Al³⁺ and (c) Fe³⁺.

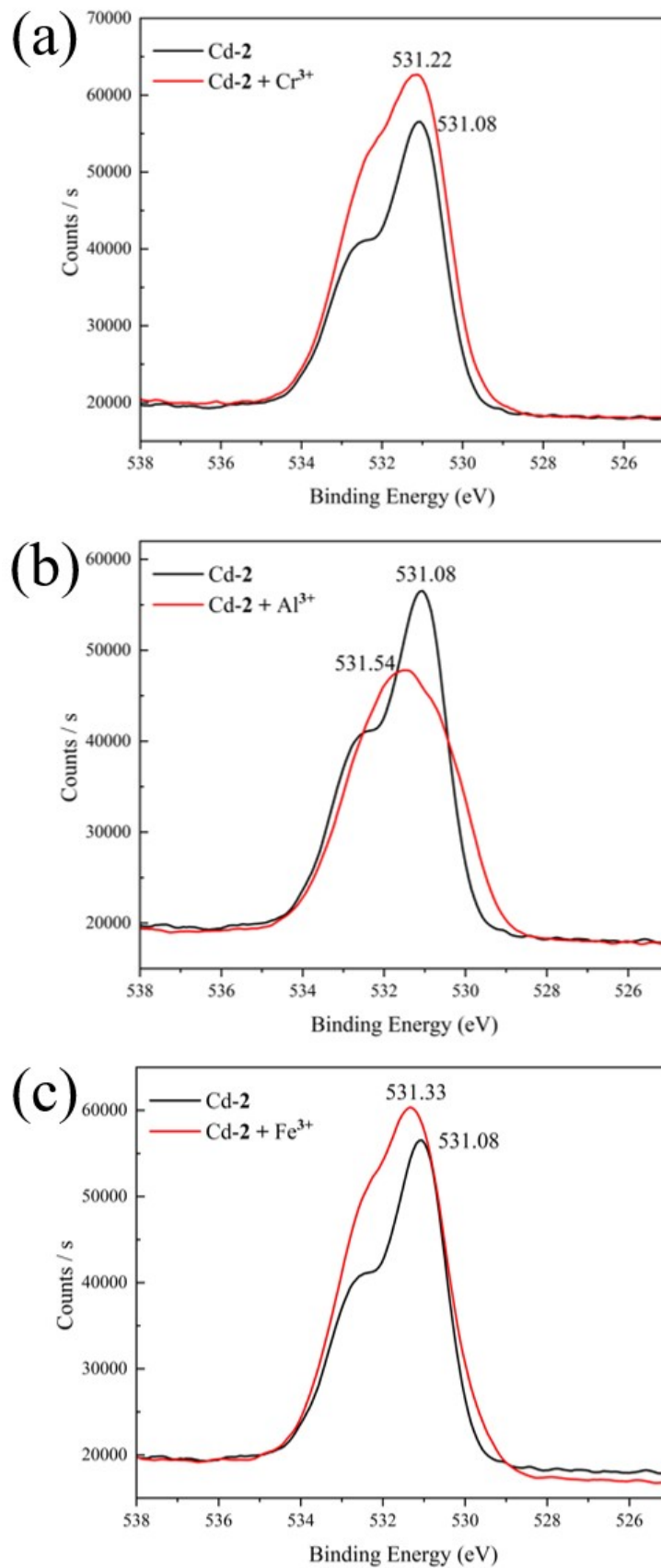


Fig. S30 XPS analysis of the O 1s peaks of **Cd-2** before and after immersed in the aqueous solution of (a) Cr³⁺, (b) Al³⁺, and (c) Fe³⁺.

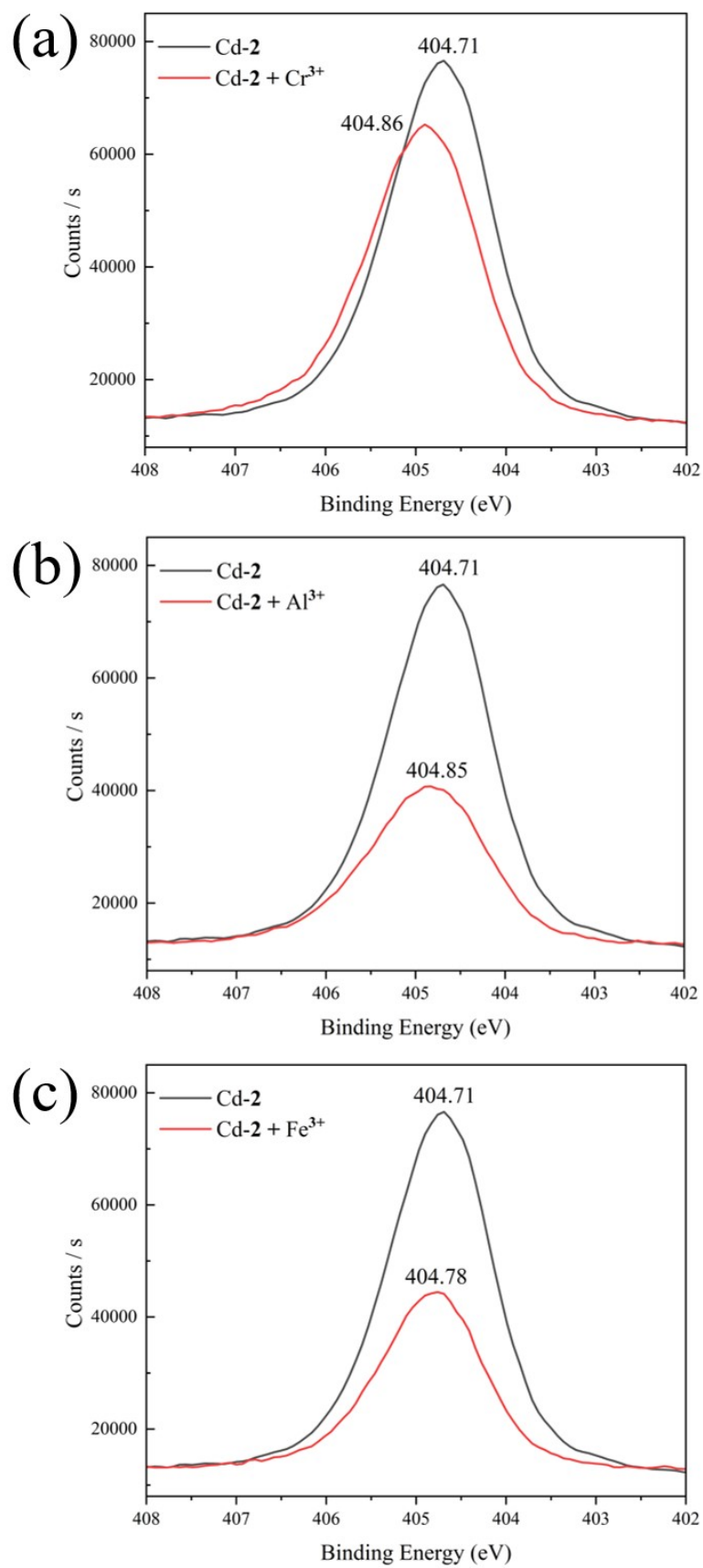


Fig. S31 XPS analysis of the N 1s peaks of **Cd-2** before and after immersed in the aqueous solution of (a) Cr³⁺, (b) Al³⁺, and (c) Fe³⁺.

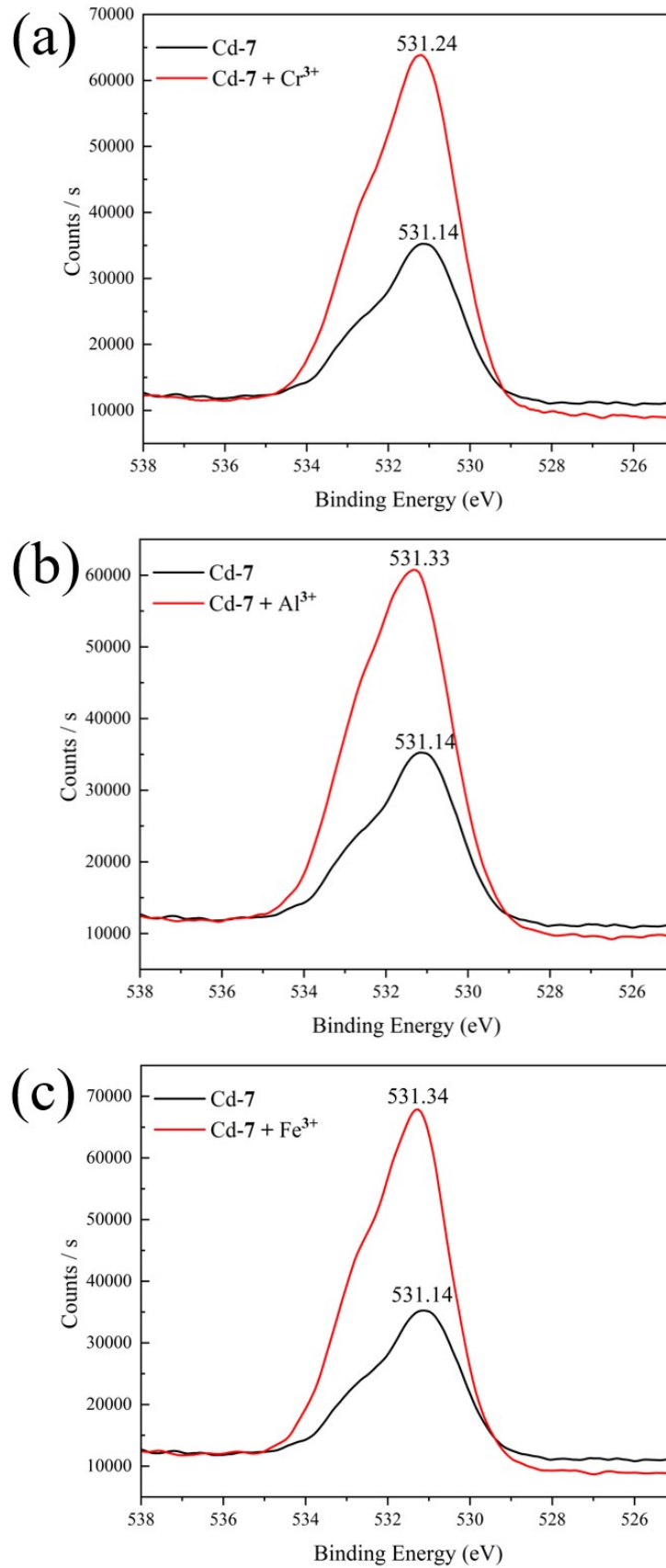


Fig. S32 XPS analysis of the O 1s peaks of **Cd-7** before and after immersed in the aqueous solution of (a) Cr³⁺, (b) Al³⁺, and (c) Fe³⁺.

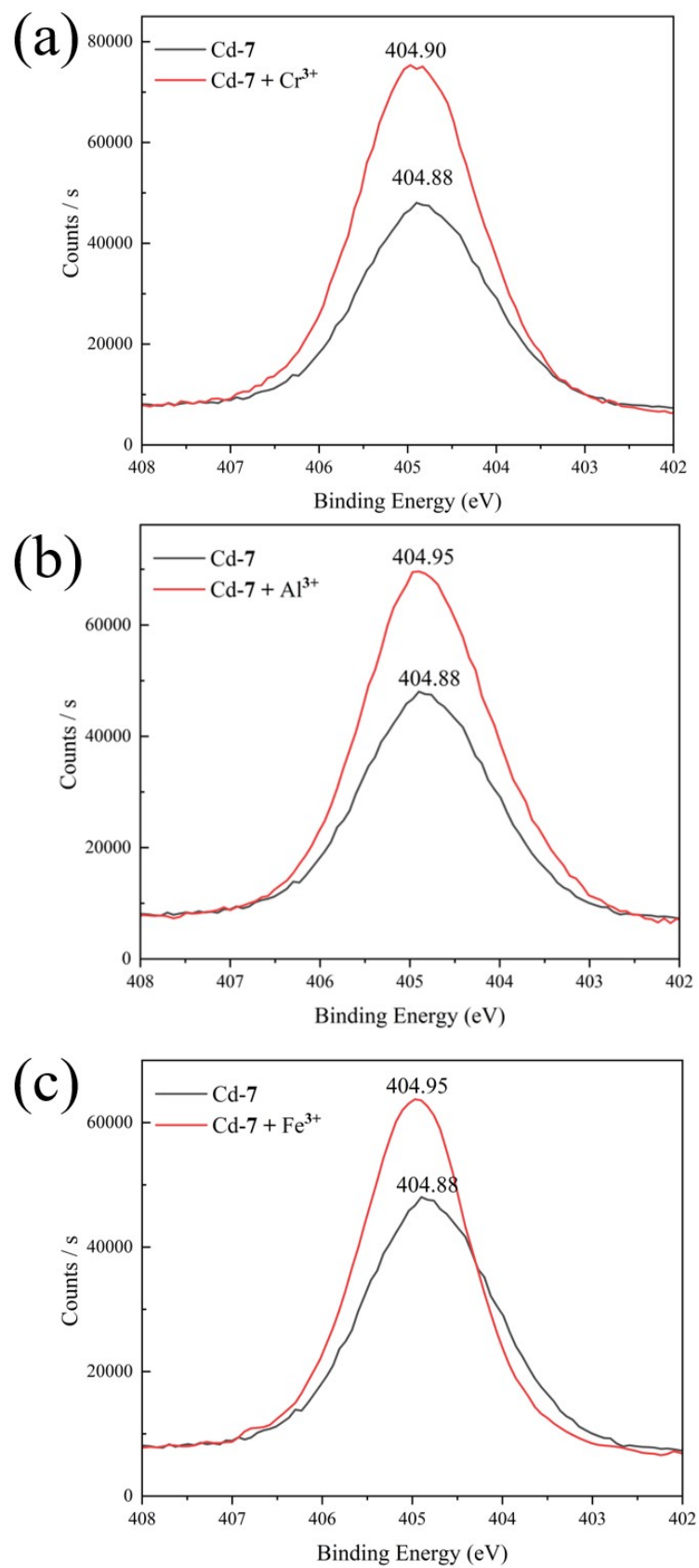


Fig. S33 XPS analysis of the N 1s peaks of **Cd-7** before and after immersed in the aqueous solution of (a) Cr³⁺, (b) Al³⁺, and (c) Fe³⁺.

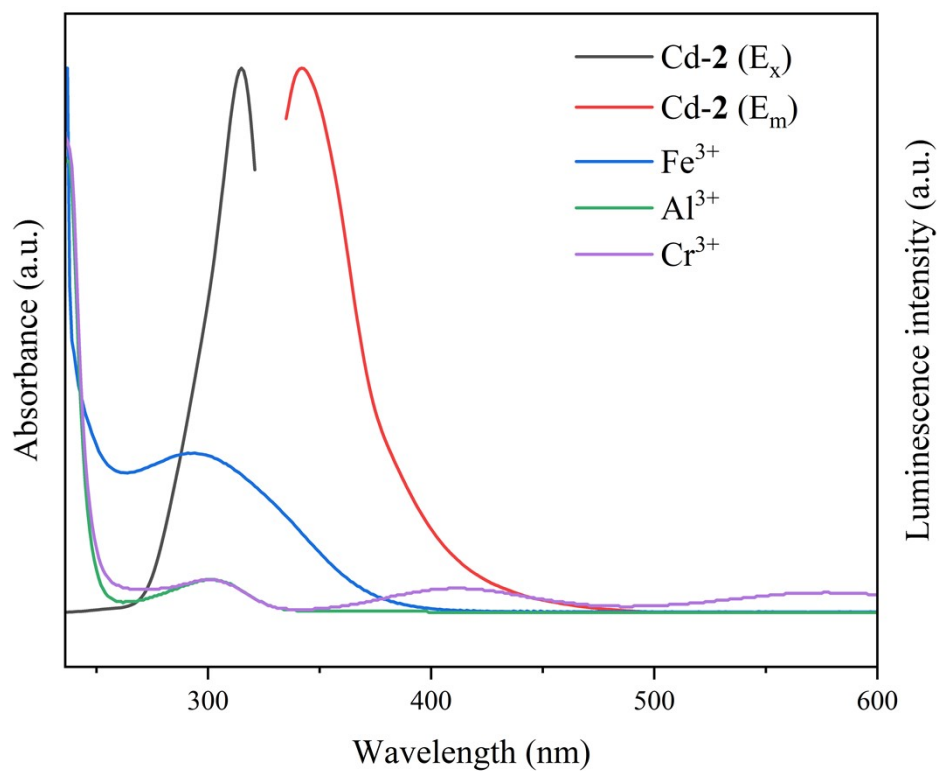


Fig. S34 Excitation and emission wavelength of Cd-2 and UV-vis absorption spectrum of Cr^{3+} , Al^{3+} , and Fe^{3+} .

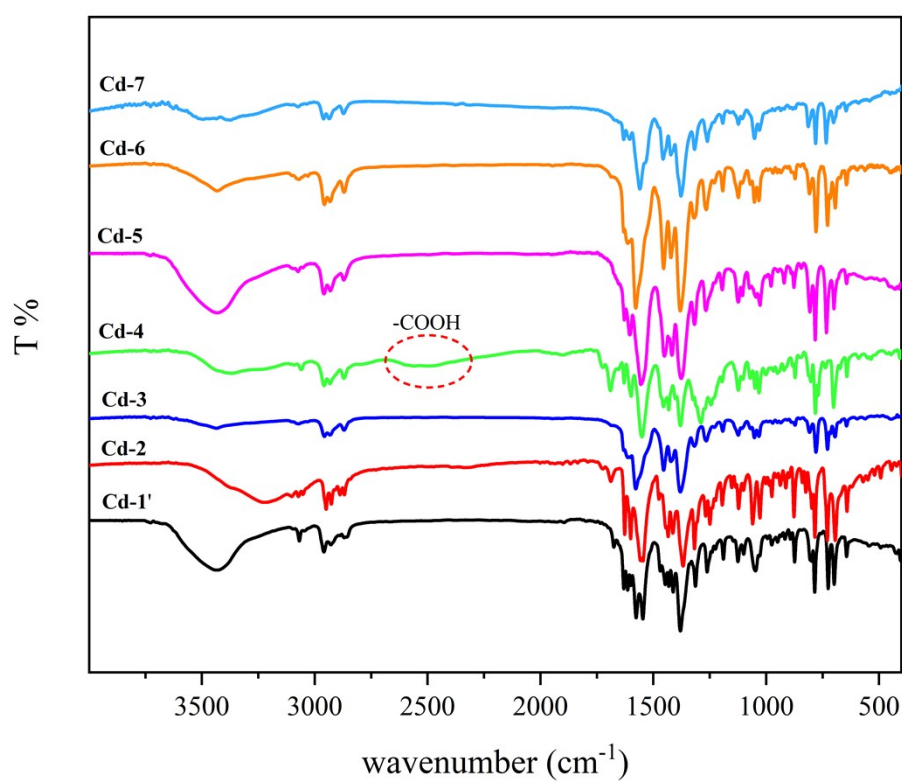


Fig. S35 FT-IR spectra of Cd-1–Cd-7.

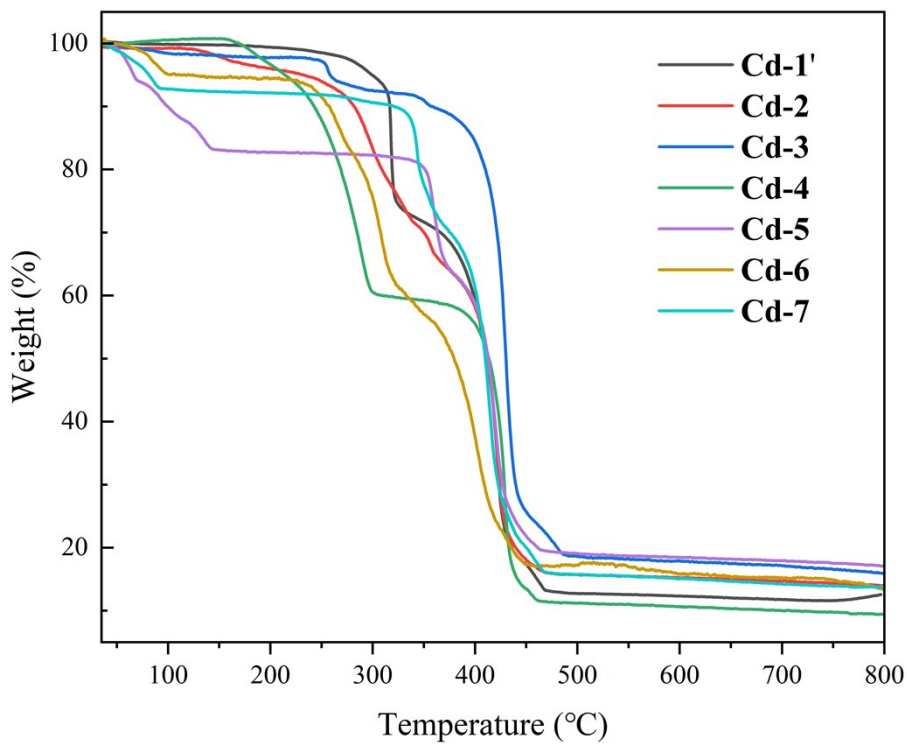


Fig. S36 TGA curves of Cd-1'–Cd-7.

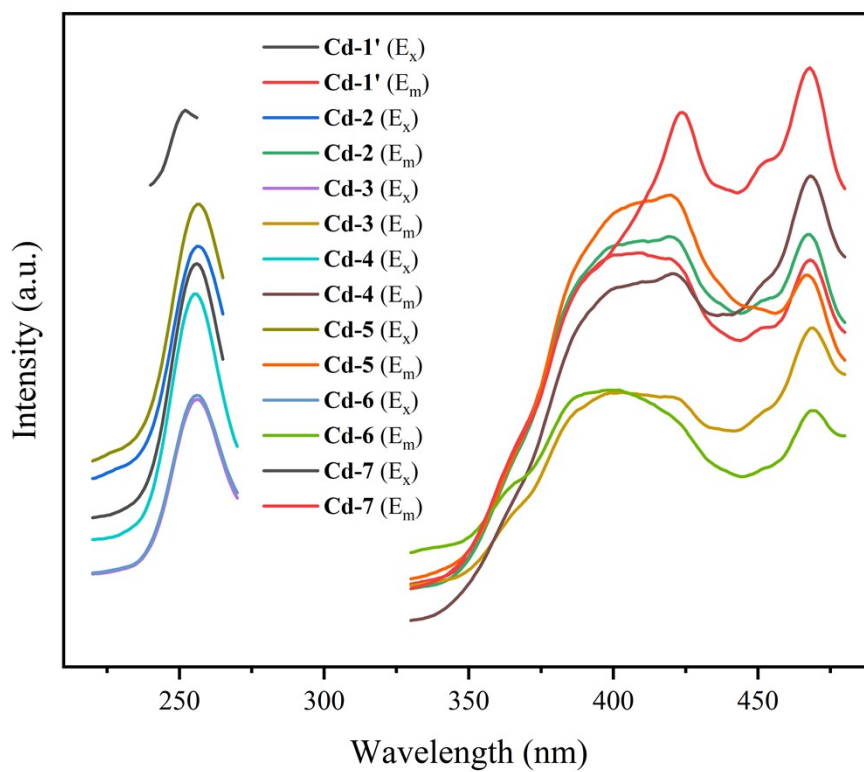
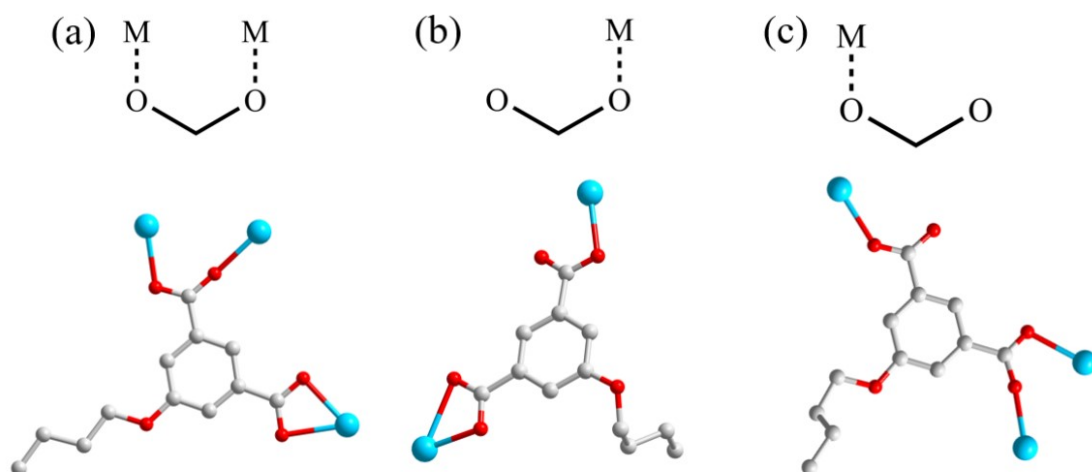
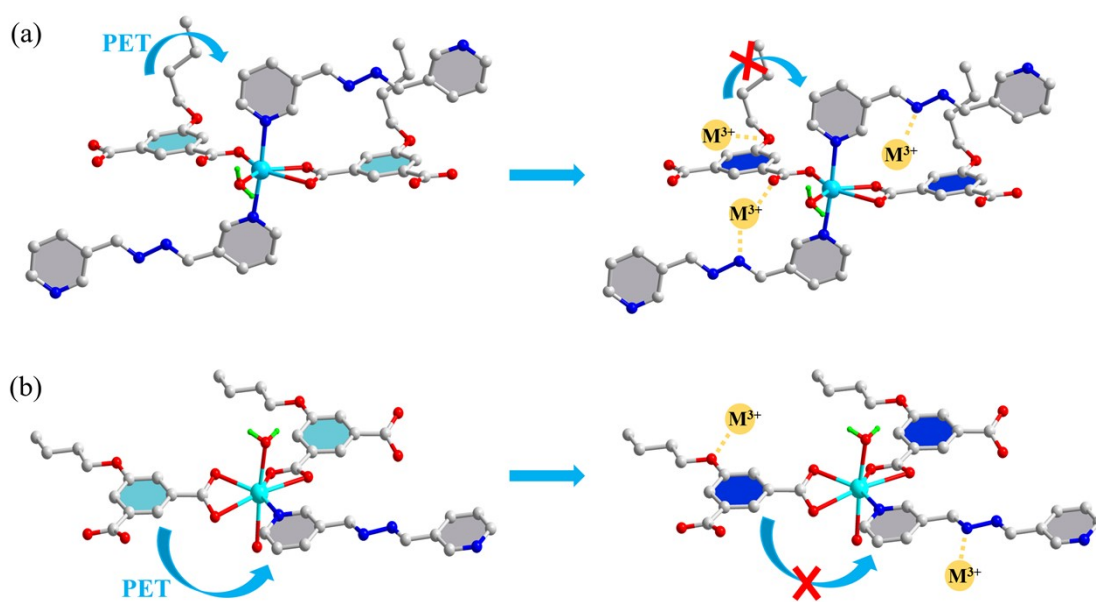


Fig. S37 Solid-state fluorescence spectra of Cd-1'–Cd-7.



Scheme S1 Coordination Modes of the *n*-BuO-*ip*²⁻ ligands in (a) **Cd-1**, (b) **Cd-2**, and (c) **Cd-3**.



Scheme S2 Schematic illustration of the PET process and the turn-on sensing of M^{3+} (Cr^{3+} , Al^{3+} , and Fe^{3+}) for (a) **Cd-2** and (b) **Cd-7**.

Table S1 Crystal data and structure refinement summary for **Cd-1–Cd-7**.

	Cd-1^a	Cd-1'^a	Cd-2
CCDC no.	2255489	2255490	2220246
empirical formula	C ₄₈ H ₄₄ Cd ₂ N ₈ O ₁₀	C ₂₄ H ₂₂ CdN ₄ O ₅	C ₂₄ H ₂₄ CdN ₄ O ₆
formula weight	1117.71	558.85	576.87
crystal system	Triclinic	Triclinic	Triclinic
space group	<i>P</i> $\bar{1}$	<i>P</i> $\bar{1}$	<i>P</i> $\bar{1}$
<i>a</i> (Å)	12.3825 (7)	10.318 (3)	8.7263 (18)
<i>b</i> (Å)	12.7510 (6)	11.477 (4)	10.387 (2)
<i>c</i> (Å)	17.7783 (8)	12.936 (5)	13.454 (3)
α (°)	82.495 (2)	111.288 (14)	94.237 (7)
β (°)	77.280 (2)	92.092 (15)	98.761 (8)
γ (°)	70.229 (2)	108.460 (11)	96.502 (7)
<i>V</i> (Å ³)	2571.9 (2)	1333.8 (8)	1192.4 (4)
<i>Z</i>	2	2	2
ρ calc (Mg m ⁻³)	1.443	1.392	1.607
μ (mm ⁻¹)	0.89	0.86	0.96
<i>F</i> (000)	1128	564	584
Radiation	Mo K α	Mo K α	Mo K α
Crystal size (mm ³)	0.14 × 0.12 × 0.06	0.14 × 0.10 × 0.04	0.27 × 0.24 × 0.2
Reflections collected	10337	24728	37941
Independent reflections	10337	4775	5911
GOF	1.031	1.023	1.068
<i>R</i> ₁ , <i>wR</i> ₂ [<i>I</i> > 2 σ (<i>I</i>)] ^b	0.0499, 0.1017	0.0700, 0.1393	0.0190, 0.0451
<i>R</i> ₁ , <i>wR</i> ₂ (all data) ^b	0.0810, 0.1127	0.1062, 0.1666	0.0211, 0.0462
$\Delta\rho_{\max}$, $\Delta\rho_{\min}$ (e Å ⁻³)	2.20, -0.89	0.69, -1.51	0.43, -0.34
	Cd-3^a	Cd-4	Cd-5
CCDC no.	2220247	2255491	2220248
empirical formula	C ₅₄ H ₅₅ Cd ₂ N ₁₀ O ₁₃	C ₆₀ H ₆₂ Cd ₂ N ₈ O ₁₇	C ₂₁ H ₂₈ CdN ₃ O ₈
formula weight	1276.88	1391.97	562.86
crystal system	Triclinic	Monoclinic	Triclinic
space group	<i>P</i> $\bar{1}$	<i>P</i> 2 ₁ / <i>c</i>	<i>P</i> $\bar{1}$
<i>a</i> (Å)	12.468 (3)	8.5651 (8)	9.2746 (4)
<i>b</i> (Å)	12.732 (3)	29.378 (3)	10.2958 (4)
<i>c</i> (Å)	18.389 (5)	24.244 (3)	14.0716 (5)
α (°)	98.114 (11)	90	73.900 (1)
β (°)	92.162 (10)	92.208 (4)	71.884 (2)
γ (°)	100.452 (9)	90	85.412 (2)
<i>V</i> (Å ³)	2836.1 (12)	6096.0 (11)	1226.96 (8)

<i>Z</i>	2	4	2
ρ calc (Mg m ⁻³)	1.495	1.517	1.524
μ (mm ⁻¹)	0.82	0.77	0.94
Radiation	Mo K α	Mo K α	Mo K α
Crystal size (mm ³)	0.2 × 0.16 × 0.15	0.24 × 0.22 × 0.2	0.3 × 0.2 × 0.16
Reflections collected	27072	12495	37385
Independent reflections	9863	12495	6094
GOF	1.033	1.075	1.050
$R_1, wR_2 [I > 2\sigma(I)]^b$	0.0465, 0.0989	0.0768, 0.1643	0.0498, 0.1109
R_1, wR_2 (all data) ^b	0.0750, 0.1094	0.1120, 0.1852	0.0756, 0.1269
$\Delta\rho_{\max}, \Delta\rho_{\min}$ (e Å ⁻³)	1.78, -0.63	1.80, -1.09	0.91, -1.42
	Cd-6	Cd-7^a	
CCDC no.	2220249	2220250	
empirical formula	C ₃₆ H ₄₄ Cd ₂ N ₄ O ₁₅	C ₁₈ H ₁₉ CdN ₂ O ₆	
formula weight	997.55	471.75	
crystal system	Triclinic	Triclinic	
space group	<i>P</i> $\bar{1}$	<i>P</i> $\bar{1}$	
<i>a</i> (Å)	10.0883 (13)	8.303 (3)	
<i>b</i> (Å)	13.3343 (17)	9.927 (4)	
<i>c</i> (Å)	14.5309 (18)	13.499 (5)	
α (°)	94.490 (5)	82.024 (15)	
β (°)	90.763 (5)	73.743 (16)	
γ (°)	99.221 (5)	66.648 (14)	
<i>V</i> (Å ³)	1922.9 (4)	980.2 (7)	
<i>Z</i>	2	2	
ρ calc (Mg m ⁻³)	1.723	1.598	
μ (mm ⁻¹)	1.18	1.15	
<i>F</i> (000)	1008	474	
Radiation	Mo K α	Mo K α	
Crystal size (mm ³)	0.26 × 0.16 × 0.14	0.2 × 0.1 × 0.08	
Reflections collected	60591	30042	
Independent reflections	9631	4887	
GOF	1.034	1.069	
$R_1, wR_2 [I > 2\sigma(I)]^b$	0.0327, 0.0675	0.0345, 0.0725	
R_1, wR_2 (all data) ^b	0.0552, 0.0767	0.0457, 0.0788	
$\Delta\rho_{\max}, \Delta\rho_{\min}$ (e Å ⁻³)	0.99, -0.86	1.37, -1.24	
^a The values in parentheses are for the refinement after the SQUEEZE routine.			
^b $R_1 = \sum F_0 - Fc / \sum F_0 $, $wR_2 = [\sum w(F_0 - Fc)^2 / \sum w(F_0)^2]^{1/2}$.			

Table S2 Selected Bond Lengths (Å) and Angles (°) for **Cd-1–Cd-7**.

Cd-1					
Cd1–O1	2.270 (3)	Cd1–O6	2.271 (3)	Cd1–O8 ^A	2.330 (3)
Cd1–O9 ^A	2.396 (3)	Cd1–N1	2.318 (4)	Cd1–N4 ^B	2.346 (4)
Cd1–C20 ^A	2.705 (4)	Cd2–O2	2.282 (3)	Cd2–O3 ^C	2.305 (3)
Cd2–O4 ^C	2.437 (3)	Cd2–O7	2.197 (3)	Cd2–N5	2.347 (4)
Cd2–N8 ^B	2.326 (4)	Cd2–C8 ^C	2.703 (4)	O1–Cd1–O6	129.35 (11)
O1–Cd1–O8 ^A	143.73 (11)	O1–Cd1–O9 ^A	88.76 (10)	O1–Cd1–N1	93.04 (13)
O1–Cd1–N4 ^B	88.82 (13)	O1–Cd1–C20 ^A	116.52 (12)	O6–Cd1–O8 ^A	86.91 (10)
O6–Cd1–O9 ^A	140.34 (11)	O6–Cd1–N1	88.59 (13)	O6–Cd1–N4 ^B	81.60 (13)
O6–Cd1–C20 ^A	113.70 (12)	O8 ^A –Cd1–O9 ^A	55.67 (10)	O8 ^A –Cd1–N4 ^B	97.07 (12)
O8 ^A –Cd1–C20 ^A	27.66 (11)	O9 ^A –Cd1–C20 ^A	28.01 (11)	N1–Cd1–O8 ^A	88.04 (12)
N1–Cd1–O9 ^A	101.41 (12)	N1–Cd1–N4 ^B	168.65 (12)	N1–Cd1–C20 ^A	95.33 (12)
N4 ^B –Cd1–O9 ^A	89.81 (11)	N4 ^B –Cd1–C20 ^A	93.84 (12)	O2–Cd2–O3 ^C	102.90 (11)
O2–Cd2–O4 ^C	155.85 (11)	O2–Cd2–N5	83.29 (12)	O2–Cd2–N8 ^B	84.84 (13)
O2–Cd2–C8 ^C	129.78 (12)	O3 ^C –Cd2–O4 ^C	55.17 (10)	O3 ^C –Cd2–N5	92.11 (12)
O3 ^C –Cd2–N8 ^B	86.87 (12)	O3 ^C –Cd2–C8 ^C	27.48 (11)	O4 ^C –Cd2–C8 ^C	27.68 (11)
O7–Cd2–O2	117.11 (11)	O7–Cd2–O3 ^C	139.91 (11)	O7–Cd2–O4 ^C	85.02 (10)
O7–Cd2–N5	90.24 (13)	O7–Cd2–N8 ^B	98.53 (13)	O7–Cd2–C8 ^C	112.58 (12)
N5–Cd2–O4 ^C	87.30 (12)	N5–Cd2–C8 ^C	89.82 (12)	N8 ^B –Cd2–O4 ^C	102.19 (12)
N8 ^B –Cd2–N5	167.55 (14)	N8 ^B –Cd2–C8 ^C	94.90 (12)		
Symmetry codes: (A) $-x+1, -y+1, -z+1$; (B) $x, y+1, z$; (C) $-x+1, -y+2, -z$.					
Cd-1'					
Cd1–O2 ^B	2.252 (5)	Cd1–O3 ^C	2.337 (5)	Cd1–O4 ^C	2.402 (6)
Cd1–O1	2.272(6)	Cd1–N4 ^A	2.349 (8)	Cd1–N1	2.325 (7)
Cd1–C20 ^C	2.709 (7)	O2 ^B –Cd1–O1	124.9 (2)	O2 ^B –Cd1–N1	92.7 (3)
O1–Cd1–N1	86.4 (3)	O2 ^B –Cd1–O3 ^C	143.8 (2)	O1–Cd1–O3 ^C	91.3 (2)
N1–Cd1–O3 ^C	87.8 (2)	O2 ^B –Cd1–N4 ^A	89.9 (3)	O1–Cd1–N4 ^A	84.6 (3)
N1–Cd1–N4 ^A	170.4 (3)	O3 ^C –Cd1–N4 ^A	95.5 (2)	O2 ^B –Cd1–O4 ^C	89.1 (2)
O1–Cd1–O4 ^C	145.3 (2)	N1–Cd1–O4 ^C	99.7 (3)	O3 ^C –Cd1–O4 ^C	55.26 (18)
N4 ^A –Cd1–O4 ^C	89.6 (3)	O2 ^B –Cd1–C20 ^C	116.6 (2)	O1–Cd1–C20 ^C	118.4 (2)
N1–Cd1–C20 ^C	93.8 (2)	O3 ^C –Cd1–C20 ^C	27.5 (2)	N4 ^A –Cd1–C20 ^C	93.2 (2)
O4 ^C –Cd1–C20 ^C	27.7 (2)				
Symmetry codes: (A) $x+1, y+1, z$; (B) $-x+3, -y+1, -z+1$; (C) $-x+2, -y+1, -z+1$.					
Cd-2					

Cd1–O1	2.2724 (11)	Cd1–O2	2.5869 (12)	Cd1–O4 ^B	2.2872 (11)
Cd1–O6	2.2805 (11)	Cd1–N1	2.3494 (13)	Cd1–N4 ^A	2.3433 (13)
O1–Cd1–O2	53.65 (4)	O1–Cd1–O4 ^B	92.19 (4)	O1–Cd1–O6	138.43 (4)
O1–Cd1–N1	90.70 (4)	O1–Cd1–N4 ^A	91.23 (4)	O4 ^B –Cd1–O2	145.82 (4)
O4 ^A –Cd1–N1	89.63 (4)	O4 ^A –Cd1–N4 ^A	85.73 (4)	O6–Cd1–O2	84.81 (4)
O6–Cd1–O4 ^B	129.37 (4)	O6–Cd1–N1	90.55 (4)	O6–Cd1–N4 ^A	91.03 (4)
N1–Cd1–O2	89.88 (4)	N4 ^A –Cd1–O2	94.94 (4)	N4 ^A –Cd1–N1	175.04 (4)

Symmetry codes: (A) $x-1, y-1, z$; (B) $x, y-1, z$.

Hydrogen-bond geometry (Å)

$D-H\cdots A$	$D-H$	$H\cdots A$	$D\cdots A$	$D-H\cdots A$
O6–H6A \cdots N3 ^E	0.88	2.01	2.8845 (17)	171
O6–H6B \cdots O3 ^F	0.88	1.85	2.6983 (14)	161

Symmetry codes: (E) $-x+1, -y+1, -z$; (F) $-x, -y+1, -z$.

Cd-3

Cd1–O6	2.361 (3)	Cd1–O10 ^A	2.347 (3)	Cd1–O2	2.289 (3)
Cd1–N9	2.425 (4)	Cd1–N1	2.366 (4)	Cd1–N4 ^B	2.368 (4)
Cd2–O8 ^C	2.323 (3)	Cd2–O7	2.283 (3)	Cd2–O3	2.259 (4)
Cd2–N8 ^D	2.289 (3)	Cd2–N5	2.273 (3)	O6–Cd1–N9	154.44 (12)
O6–Cd1–N1	90.37 (13)	O6–Cd1–N4 ^B	92.71 (13)	O10 ^A –Cd1–O6	79.48 (12)
O10 ^A –Cd1–N9	76.26 (12)	O10 ^A –Cd1–N1	91.28 (12)	O10 ^A –Cd1–N4 ^B	86.53 (12)
O2–Cd1–O6	80.66 (13)	O2–Cd1–O10 ^A	159.90 (13)	O2–Cd1–N9	123.84 (13)
O2–Cd1–N1	91.92 (12)	O2–Cd1–N4 ^B	91.35 (12)	N1–Cd1–N9	82.29 (14)
N1–Cd1–N4 ^B	175.83 (14)	N4 ^B –Cd1–N9	93.74 (14)	O7–Cd2–O8 ^C	127.26 (14)
O7–Cd2–N8 ^D	85.06 (12)	O3–Cd2–O8 ^C	80.44 (13)	O3–Cd2–O7	152.29 (13)
O3–Cd2–N8 ^D	93.01 (13)	O3–Cd2–N5	92.32 (13)	N8 ^D –Cd2–O8 ^C	93.84 (13)
N5–Cd2–O8 ^C	92.91 (13)	N5–Cd2–O7	87.45 (12)	N5–Cd2–N8 ^D	172.01 (13)

Symmetry codes: (A) $x-1, y+1, z$; (B) $x, y+1, z$; (C) $-x+1, -y+1, -z$; (D) $x-1, y, z$.

Hydrogen-bond geometry (Å)

$D-H\cdots A$	$D-H$	$H\cdots A$	$D\cdots A$	$D-H\cdots A$
O6–H6A \cdots O9 ^A	0.87	1.88	2.675 (4)	150
O6–H6B \cdots O12	0.88	2.03	2.825 (5)	150
O12–H12A \cdots O9 ^C	0.87	1.98	2.845 (6)	174
O12–H12B \cdots O13	0.87	1.96	2.823 (6)	171
O13–H13A \cdots O3	0.87	2.07	2.859 (6)	150
O13–H13B \cdots O8 ^C	0.87	2.19	2.858 (7)	134

Symmetry codes: (A) $x-1, y+1, z$; (C) $-x+1, -y+1, -z$.					
Cd-4					
Cd1–O1	2.235 (6)	Cd1–O6	2.454 (6)	Cd1–O7	2.366 (7)
Cd1–O11	2.271 (7)	Cd1–N1	2.326 (8)	Cd1–N8 ^A	2.337 (8)
Cd1–C13	2.748 (10)	Cd2–O17	2.279 (7)	Cd2–O3	2.265 (6)
Cd2–O12	2.396 (6)	Cd2–O13	2.402 (7)	Cd2–N4 ^A	2.328 (8)
Cd2–N5	2.331 (8)	Cd2–C25	2.709 (10)	O1–Cd1–O6	109.4 (2)
O1–Cd1–O7	162.2 (2)	O1–Cd1–O11	117.0 (2)	O1–Cd1–N1	89.2 (3)
O1–Cd1–N8 ^A	85.5 (3)	O1–Cd1–C13	136.0 (3)	O6–Cd1–C13	26.8 (3)
O7–Cd1–O6	54.4 (2)	O7–Cd1–C13	27.7 (3)	O11–Cd1–O6	132.7 (2)
O11–Cd1–O7	80.4 (2)	O11–Cd1–N1	91.4 (3)	O11–Cd1–N8 ^A	100.0 (3)
O11–Cd1–C13	106.8 (3)	N1–Cd1–O6	79.9 (3)	N1–Cd1–O7	94.1 (3)
N1–Cd1–N8 ^A	168.6 (3)	N1–Cd1–C13	85.2 (3)	N8 ^A –Cd1–O6	92.3 (3)
N8 ^A –Cd1–O7	88.0 (3)	N8 ^A –Cd1–C13	91.6 (3)	O17–Cd2–O12	134.7 (2)
O17–Cd2–O13	80.9 (2)	O17–Cd2–N4 ^A	92.6 (3)	O17–Cd2–N5	101.3 (3)
O17–Cd2–C25	108.0 (3)	O3–Cd2–O17	117.3 (2)	O3–Cd2–O12	107.5 (2)
O3–Cd2–O13	161.7 (2)	O3–Cd2–N4 ^A	89.6 (3)	O3–Cd2–N5	85.7 (3)
O3–Cd2–C25	134.6 (3)	O12–Cd2–O13	54.9 (2)	O12–Cd2–C25	27.1 (3)
O13–Cd2–C25	27.8 (3)	N4 ^A –Cd2–O12	81.2 (2)	N4 ^A –Cd2–O13	92.2 (3)
N4 ^A –Cd2–N5	166.0 (3)	N4 ^A –Cd2–C25	84.9 (3)	N5–Cd2–O12	87.6 (3)
N5–Cd2–O13	88.3 (3)	N5–Cd2–C25	89.0 (3)		
Symmetry codes: (A) $x+1, y, z$; (B) $x-1, y, z$.					
Hydrogen-bond geometry (Å)					
$D-H\cdots A$	$D-H$	$H\cdots A$	$D\cdots A$	$D-H\cdots A$	
O17–H17A \cdots O7 ^C	0.87	1.84	2.690 (10)	164	
O17–H17B \cdots O9 ^D	0.87	2.01	2.777 (9)	147	
O10–H10 \cdots O4 ^E	0.84	1.71	2.530 (9)	165	
O11–H11A \cdots O13 ^F	0.87	1.87	2.720 (10)	166	
O11–H11B \cdots O14 ^D	0.87	1.98	2.739 (10)	146	
O15–H15 \cdots O2 ^E	0.84	1.73	2.565 (10)	170	
Symmetry code: (C) $-x+1, y-1/2, -z+3/2$; (D) $x, -y+1/2, z-1/2$; (E) $x, -y+1/2, z+1/2$; (F) $-x+1, y+1/2, -z+3/2$.					
Cd-5					
Cd1–N1	2.324 (4)	Cd1–O4 ^A	2.367 (3)	Cd1–O5 ^A	2.443 (3)
Cd1–O1	2.228 (3)	Cd1–O6	2.369 (4)	Cd1–O7	2.283 (4)
Cd1–C17 ^A	2.753 (4)	N1–Cd1–O4 ^A	135.62 (12)	N1–Cd1–O5 ^A	82.61 (11)

N1–Cd1–O6	84.07 (15)	N1–Cd1–C17 ^A	109.13 (12)	O1–Cd1–N1	135.33 (12)
O1–Cd1–O4 ^A	88.18 (11)	O1–Cd1–O5 ^A	141.98 (11)	O1–Cd1–O6	90.93 (15)
O1–Cd1–O7	86.47 (13)	O1–Cd1–C17 ^A	115.02 (11)	O4 ^A –Cd1–O5 ^A	53.98 (10)
O4 ^A –Cd1–C17 ^A	26.84 (10)	O5 ^A –Cd1–C17 ^A	27.20 (10)	O6–Cd1–O4 ^A	87.60 (15)
O6–Cd1–O5 ^A	91.03 (14)	O6–Cd1–C17 ^A	87.90 (14)	O7–Cd1–N1	92.01 (13)
O7–Cd1–O4 ^A	100.51 (13)	O7–Cd1–O5 ^A	96.09 (12)	O7–Cd1–O6	171.38 (14)
O7–Cd1–C17 ^A	100.65 (12)				
Symmetry codes: (A) $x, y-1, z$.					
Hydrogen-bond geometry (Å)					
<i>D–H···A</i>	<i>D–H</i>	<i>H···A</i>	<i>D···A</i>	<i>D–H···A</i>	
O7–H7A···O5 ^D	0.85	1.88	2.702 (4)	163	
O7–H7B···O8	0.85	1.91	2.706 (5)	154	
O8–H8D···O2 ^D	0.85	1.92	2.753 (5)	168	
Symmetry code: (D) $-x+1, -y+1, -z+1$.					
Cd-6					
Cd1–O1	2.2567 (18)	Cd1–O6	2.2967 (19)	Cd1–O7	2.276 (2)
Cd1–O10 ^A	2.3947 (18)	Cd1–O11 ^A	2.437 (2)	Cd1–N1	2.315 (2)
Cd2–O3 ^B	2.4417 (18)	Cd2–O4 ^B	2.386 (2)	Cd2–O8	2.4916 (18)
Cd2–O9	2.3444 (18)	Cd2–O13	2.340 (2)	Cd2–O14	2.2946 (19)
Cd2–N4	2.332 (2)	O1–Cd1–O6	86.38 (7)	O1–Cd1–O7	137.70 (7)
O1–Cd1–O10 ^A	136.74 (7)	O1–Cd1–O11 ^A	83.41 (7)	O1–Cd1–N1	92.59 (7)
O6–Cd1–O10 ^A	87.10 (8)	O6–Cd1–O11 ^A	89.52 (7)	O6–Cd1–N1	177.23 (8)
O7–Cd1–O6	83.84 (7)	O7–Cd1–O10 ^A	83.74 (7)	O7–Cd1–O11 ^A	137.35 (6)
O7–Cd1–N1	95.23 (8)	O10 ^A –Cd1–O11 ^A	53.81 (6)	N1–Cd1–O10 ^A	95.40 (8)
N1–Cd1–O11 ^A	92.91 (8)	O3 ^B –Cd2–O8	168.54 (7)	O4 ^B –Cd2–O3 ^B	54.10 (7)
O4 ^B –Cd2–O8	134.59 (6)	O9–Cd2–O3 ^B	132.22 (7)	O9–Cd2–O4 ^B	80.97 (6)
O9–Cd2–O8	54.05 (6)	O13–Cd2–O3 ^B	79.14 (7)	O13–Cd2–O4 ^B	129.45 (7)
O13–Cd2–O8	94.66 (7)	O13–Cd2–O9	148.53 (7)	O14–Cd2–O3 ^B	80.57 (7)
O14–Cd2–O4 ^B	94.83 (7)	O14–Cd2–O8	90.51 (7)	O14–Cd2–O9	88.87 (7)
O14–Cd2–O13	95.31 (8)	O14–Cd2–N4	173.09 (7)	N4–Cd2–O3 ^B	105.38 (7)
N4–Cd2–O4 ^B	91.57 (8)	N4–Cd2–O8	83.13 (7)	N4–Cd2–O9	89.56 (7)
N4–Cd2–O13	82.57 (9)	C1–O1–Cd1	105.56 (17)	C8–O3–Cd2 ^B	91.19 (15)
Symmetry codes: (A) $-x+2, -y+2, -z+1$; (B) $-x+1, -y+1, -z$.					
Hydrogen-bond geometry (Å)					
<i>D–H···A</i>	<i>D–H</i>	<i>H···A</i>	<i>D···A</i>	<i>D–H···A</i>	

O6–H6A···O1 ^C	0.88	1.90	2.729 (3)	157	
O6–H6B···O11 ^D	0.88	1.94	2.743 (3)	153	
O7–H7A···O2 ^E	0.88	1.89	2.659 (3)	146	
O13–H13A···O8 ^F	0.87	1.89	2.734 (3)	162	
O14–H14A···O4 ^G	0.87	1.89	2.725 (3)	161	
O14–H14B···O9 ^H	0.87	2.08	2.832 (3)	143	
O15–H15A···O10 ^I	0.87	1.84	2.663 (3)	157	
O15–H15B···O3	0.87	1.87	2.686 (3)	156	
Symmetry codes: (C) $-x+3, -y+1, -z+1$; (D) $x+1, y-1, z$; (E) $-x+2, -y+1, -z+1$; (F) $-x+1, -y+2, -z$; (G) $x-1, y+1, z$; (H) $-x, -y+2, -z$; (I) $x, y-1, z$.					
Cd-7					
Cd1–O1	2.583 (2)	Cd1–O2	2.263 (2)	Cd1–O3 ^A	2.515 (2)
Cd1–O3 ^B	2.419 (2)	Cd1–O4 ^A	2.331 (2)	Cd1–O6	2.357 (2)
Cd1–N1	2.294 (3)	O2–Cd1–O1	53.83 (7)	O2–Cd1–O3 ^B	91.72 (8)
O2–Cd1–O3 ^A	130.53 (7)	O2–Cd1–O4 ^A	85.47 (7)	O2–Cd1–O6	90.79 (8)
O2–Cd1–N1	141.51 (8)	O3 ^A –Cd1–O1	171.55 (6)	O3 ^B –Cd1–O1	100.20 (7)
O3 ^B –Cd1–O3 ^A	73.32 (8)	O4 ^A –Cd1–O1	133.87 (7)	O4 ^A –Cd1–O3 ^B	101.91 (7)
O4 ^A –Cd1–O3 ^A	53.98 (7)	O4 ^A –Cd1–O6	83.84 (8)	O6–Cd1–O1	76.86 (8)
O6–Cd1–O3 ^B	173.89 (7)	O6–Cd1–O3 ^A	109.06 (8)	N1–Cd1–O1	88.63 (8)
N1–Cd1–O3 ^B	86.56 (8)	N1–Cd1–O3 ^A	85.61 (8)	N1–Cd1–O4 ^A	132.49 (8)
N1–Cd1–O6	88.01 (8)				
Symmetry codes: (A) $x+1, y-1, z$; (B) $-x+1, -y+1, -z+1$.					

Table S3 SCSC transformation conditions.

Sample	DMF/mL	H ₂ O/mL	Other stimulating	Time	Temperature/°C	result			
Cd-1'	0.1	1.9		7 days	RT	×			
	0.2	1.8				×			
	0.3	1.7				Cd-2			
	0.4	1.6				×			
	0.5	1.5				×			
	0.6	1.4				×			
	0.7	1.3				×			
	0.8	1.2				×			
	0.9	1.1				×			
	1	1				×			
		2	stirring	14 days		Cd-5			
Cd-5	0.1	1.9		16 days		Cd-3			
	0.2	1.8				Cd-6			
	0.3	1.7				×			
	0.4	1.6				Cd-2			
	0.5	1.5				×			
	0.6	1.4				×			
	0.7	1.3				×			
	0.8	1.2				×			
	0.9	1.1				×			
	1	1				×			
		2					0.5 hour		Cd-7
		vapor				98% humidity	4 hours	25	Cd-7
	Cd-2	1.2	0.8		2 days	105	×		
1.4		0.6	×						
1.6		0.4	×						
1.8		0.2	×						
1		1	Cd-5						
1		1		7 days	RT	×			

Table S4 Comparison of the ground state energies and the transformation energyfor Cd-CPs calculated at B3LYP/LANL2DZ² level.

Compounds	<i>n</i> -BuO-ip	3-bpdb	DMF	water
Relative ground state energy × 10 ⁵ [kcal/mol]	-5.2732	-2.1391	-1.55826	-0.47892
Compounds	Cd	Cd-1'	Cd-2	Cd-3
Relative ground state energy × 10 ⁵ [kcal/mol]	-0.3017	-9.8531	-10.3337	-24.4678
Compounds	Cd-5	Cd-6	Cd-7	
Relative ground state energy × 10 ⁵ [kcal/mol]	-11.8909	-17.3469	-10.334	
Transformation	Cd-1'→Cd-2	Cd-1'→Cd-3	Cd-1'→Cd-5	Cd-2↔Cd-5
Δ Energy [kcal/mol]	-162.7096	-48315.9070	-61.23243	±101.4772
Transformation	Cd-5→Cd-6	Cd-5→Cd-7		
Δ Energy [kcal/mol]	-252.84207	-100.8729		

Table S5 Fluorescent sensor for Cr³⁺ and Al³⁺ detection based on various CPs.

CPs	ions	Fluorescent response	LOD	Ref.
[Zn(4-nvp) ₂ (SCN) ₂]	Cr ³⁺	Enhancement	2.53 μM	17
[Zn(4-nvp) ₂ (SCN) ₂]	Al ³⁺	Enhancement	2.67 μM	17
{[(CH ₃) ₂ NH ₂][Eu-(BTDB) ₂ ·2H ₂ O] _n }	Al ³⁺	Enhancement	2.9 ppm	18
{[Co ₃ (BIBT) ₃ (BTC) ₂ (H ₂ O) ₂]·solvents _n }	Cr ³⁺	Enhancement	0.10 μM	19
{[Co ₃ (BIBT) ₃ (BTC) ₂ (H ₂ O) ₂]·solvents _n }	Al ³⁺	Enhancement	0.10 μM	19
Zn(DMA)(TBA)	Al ³⁺	Enhancement	1.97 μM	20
[Cd(NH ₂ -bdc)(azp)]·DMF	Cr ³⁺	Enhancement	0.6 μM	21
Cd-2	Cr ³⁺	Enhancement	5.52 μM	This work
Cd-2	Al ³⁺	Enhancement	2.60 μM	This work
Cd-7	Cr ³⁺	Enhancement	9.84 μM	This work
Cd-7	Al ³⁺	Enhancement	8.90 μM	This work
[Tb(ppda)(ox) _{0.5} (H ₂ O) ₂] _n	Al ³⁺	Quenching	5.66 μM	22
{[Ba ₃ La _{0.5} (μ ₃ -L) _{2.5} (H ₂ O) ₃ (DMF)]·(3DMF) _n }	Al ³⁺	Quenching	1.11 μM	23
{[Cd ₂ (SA) ₂ (L) ₂]·H ₂ O} _n	Al ³⁺	Quenching	93 μM	24
[Cd(CDC)(L)] _n	Al ³⁺	Quenching	61 μM	24
Zn ₃ (bpdc) ₂ (pdc)(DMF)·6DMF	Cr ³⁺	Quenching	25.1 μM	25

References

1. S. Shanmuga Sundara Raj, H.-K. Fun, J. Zhang, R.-G. Xiong and X.-Z. You, Pyridine-4-carbaldehyde azine, *Acta Crystallographica Section C*, 2000, **56**, e274-e275.
2. A. J. Guenther, M. C. Davis, M. D. Ford, J. T. Reams, T. J. Groshens, L. C. Baldwin, L. M. Lubin and J. M. Mabry, Polycyanurate Networks with Enhanced Segmental Flexibility and Outstanding Thermochemical Stability, *Macromolecules*, 2012, **45**, 9707-9718.
3. V. A. Blatov, A. P. Shevchenko and D. M. Proserpio, Applied Topological Analysis of Crystal Structures with the Program Package ToposPro, *Crystal Growth & Design*, 2014, **14**, 3576-3586.
4. APEX3 is Bruker's comprehensive software suite for single-crystal X-ray diffraction which combined with Bruker's X-ray diffractometer systems, and provides the tools for complete small-molecule structure determination.
5. Bruker. SAINT+, Bruker AXS Inc., Madison, Wisconsin, USA, 2007.
6. G. M. Sheldrick, Crystal structure refinement with SHELXL, *Acta Crystallographica Section C Structural Chemistry*, 2015, **71**, 3-8.
7. O. V. Dolomanov, L. J. Bourhis, R. J. Gildea, J. A. K. Howard and H. Puschmann, OLEX2: a complete structure solution, refinement and analysis program, *Journal of Applied Crystallography*, 2009, **42**, 339-341.
8. G. Sheldrick, SHELXT - Integrated space-group and crystal-structure determination, *Acta Crystallographica Section A*, 2015, **71**, 3-8.
9. A. Spek, PLATON SQUEEZE: a tool for the calculation of the disordered solvent contribution to the calculated structure factors, *Acta Crystallographica Section C*, 2015, **71**, 9-18.
10. S.-S. Chen, Z.-Y. Zhang, R.-B. Liao, Y. Zhao, C. Wang, R. Qiao and Z.-D. Liu, A Photoluminescent Cd(II) Coordination Polymer with Potential Active Sites Exhibiting Multiresponsive Fluorescence Sensing for Trace Amounts of NACs and Fe³⁺ and Al³⁺ Ions, *Inorganic Chemistry*, 2021, **60**, 4945-4956.
11. H.-Y. Lin, J. Luan, X.-L. Wang, G.-C. Liu and J.-W. Zhang, Three Transition Metal(II) Coordination Polymers Constructed by a Semi-rigid Bis-pyridyl-bis-amide and Dicarboxylates Mixed Ligands: Assembly, Structures and Properties, *Zeitschrift für anorganische und allgemeine Chemie*, 2014, **640**, 2041-2048.
12. R. Pal, M. B. Reddy, B. Dinesh, P. Balaram and T. N. Guru Row, Temperature-induced reversible first-order single crystal to single crystal phase transition in Boc-gamma(4)(R)Val-Val-OH: interplay of enthalpy and entropy, *J Phys Chem A*, 2014, **118**, 9568-9574.
13. J. Zhao, J. Yuan, Z. Fang, S. Huang, Z. Chen, F. Qiu, C. Lu, J. Zhu and X. Zhuang, One-dimensional coordination polymers based on metal-nitrogen linkages, *Coordination Chemistry Reviews*, 2022, **471**.
14. W. L. Leong and J. J. Vittal, One-Dimensional Coordination Polymers: Complexity and Diversity in Structures, Properties, and Applications, *Chemical Reviews*, 2011, **111**, 688-764.
15. A. Goswami, S. Sengupta and R. Mondal, Construction of helical networks by using multiple V-shaped mixed ligand systems, *CrystEngComm*, 2012, **14**, 561-572.

16. C. Ma, C. Chen, Q. Liu, F. Chen, D. Liao, L. Li and L. Sun, Synthesis, Structure and Magnetic Properties of a Series of Novel Isophthalate-Bridged Manganese (II) Polymers with Double-Layer or Double-Chain Structures, *European Journal of Inorganic Chemistry*, 2004, **2004**, 3316-3325.
17. B. Dutta, S. Dey, K. Pal, S. Bera, S. Naaz, K. Jana, C. Sinha and M. H. Mir, Supramolecular assembly of a 4-(1-naphthylvinyl)pyridine-appended Zn(ii) coordination compound for the turn-on fluorescence sensing of trivalent metal ions (Fe^{3+} , Al^{3+} , and Cr^{3+}) and cell imaging application, *New Journal of Chemistry*, 2020, **44**, 13163-13171.
18. J. Li, Y. Zhu, H. Xu, T. F. Zheng, S. J. Liu, Y. Wu, J. L. Chen, Y. Q. Chen and H. R. Wen, A Benzothiadiazole-Based Eu(3+) Metal-Organic Framework as the Turn-On Luminescent Sensor toward Al(3+) and Ga(3+) with Potential Bioimaging Application, *Inorg Chem*, 2022, **61**, 3607-3615.
19. X. M. Tian, S. L. Yao, C. Q. Qiu, T. F. Zheng, Y. Q. Chen, H. Huang, J. L. Chen, S. J. Liu and H. R. Wen, Turn-On Luminescent Sensor toward Fe(3+), Cr(3+), and Al(3+) Based on a Co(II) Metal-Organic Framework with Open Functional Sites, *Inorg Chem*, 2020, **59**, 2803-2810.
20. X. Zhang, X. Luo, N. Zhang, J. Wu and Y.-Q. Huang, A highly selective and sensitive Zn(ii) coordination polymer luminescent sensor for Al^{3+} and NACs in the aqueous phase, *Inorganic Chemistry Frontiers*, 2017, **4**, 1888-1894.
21. T. Wiwasuku, J. Boonmak, R. Burakham, S. Hadsadee, S. Jungsuttiwong, S. Bureekaew, V. Promarak and S. Youngme, Turn-on fluorescent probe towards glyphosate and Cr^{3+} based on Cd(ii)-metal organic framework with Lewis basic sites, *Inorganic Chemistry Frontiers*, 2021, **8**, 977-988.
22. Z. Zhan, Y. Jia, D. Li, X. Zhang and M. Hu, A water-stable terbium-MOF sensor for the selective, sensitive, and recyclable detection of Al(3+) and CO_3^{2-} ions, *Dalton Trans*, 2019, **48**, 15255-15262.
23. B. Ding, S. X. Liu, Y. Cheng, C. Guo, X. X. Wu, J. H. Guo, Y. Y. Liu and Y. Li, Heterometallic Alkaline Earth-Lanthanide Ba(II)-La(III) Microporous Metal-Organic Framework as Bifunctional Luminescent Probes of Al(3+) and MnO_4^- , *Inorg Chem*, 2016, **55**, 4391-4402.
24. S. Chand, M. Mondal, S. C. Pal, A. Pal, S. Maji, D. Mandal and M. C. Das, Two azo-functionalized luminescent 3D Cd(ii) MOFs for highly selective detection of Fe^{3+} and Al^{3+} , *New Journal of Chemistry*, 2018, **42**, 12865-12871.
25. X. Meng, M. J. Wei, H. N. Wang, H. Y. Zang and Z. Y. Zhou, Multifunctional luminescent Zn(ii)-based metal-organic framework for high proton-conductivity and detection of Cr^{3+} ions in the presence of mixed metal ions, *Dalton Trans*, 2018, **47**, 1383-1387.